Piecewise-stationary motion modeling and iterative smoothing to track heterogeneous particle motions in dense environments

Philippe Roudot, Liya Ding, Khuloud Jaqaman, Charles Kervrann, Gaudenz Danuser

Piecewise-stationary motion modeling and iterative smoothing to track heterogeneous particle motions in dense environments

Philippe Roudot, Liya Ding, Khuloud Jaqaman, Charles Kervrann, Gaudenz Danuser

***Abstract*— One of the major challenges in multiple particle tracking is the capture of extremely heterogeneous movements of objects in crowded scenes. The presence of numerous assignment candidates in the expected range of particle motion makes the tracking ambiguous and induces false positives. Lowering the ambiguity by reducing the search range, on the other hand, is not an option, as this would increase the rate of false negatives. We propose here a piecewise-stationary motion model (PMM) for the particle transport along an iterative smoother that exploits recursive tracking in multiple rounds in forward and backward temporal directions. By fusing past and future information, our method, termed PMMS, can recover fast transitions from freely or confined diffusive to directed motions with linear time complexity. To avoid false positives we complemented recursive tracking with a robust inline estimator of the search radius for assignment (a.k.a. gating), where past and future information are exploited using only two frames at each optimization step. We demonstrate the improvement of our technique on simulated data – especially the impact of density, variation in frame to frame displacements, and motion switching probability. We evaluated our technique on the 2D particle tracking challenge dataset published by Chenouard *et al* in 2014. Using high SNR to focus on motion modeling challenges, we show superior performance at high particle density. On biological applications, our algorithm allows us to quantify the extremely small percentage of motor-driven movements of fluorescent particles along microtubules in a dense field of unbound, diffusing particles. We also show with virus imaging that our algorithm can cope with a strong reduction in recording frame rate while keeping the same performance relative to methods relying on fast sampling.**

***Index Terms*— Multiple particle tracking (MPT), Cell biology, Interacting multiple model, Kalman smoothing, Adaptive gating.**

I. Introduction

Image tracking of fluorescent objects, from labeled molecules, to organelles, and entire cells is an essential task in the analysis of cellular functions. Inspired by automatic tracking algorithms proposed for applications in aerospatial or street surveillance [1], the tracking of particles in molecular bioimaging has been a focus of many studies [2]. [1]

A good number of challenges faced by the quantification of intracellular dynamics have been tackled by automatic methods. Assignment in a group of detected particles in close proximity is handled by combinatorial optimization in a fixed time window ranging from frame-to-frame association [3]–[5] to considering groups of frames [6]–[10] and batch algorithms that employ more complex graph pruning techniques [11], [12]. Intracellular transport modeling has been carried out using Bayesian filtering [13], [3], [14], [15]. Transient disappearances, object misdetection and particle merging have been recovered by either considering link cost minimization on a group of frames for optimization [6], [7], [8] or using a post-processing step applied on tracklets [3]. Particle detection and linking is an efficient framework to estimate trajectories when the signal-to-noise ratio (SNR) is sufficient, lower SNR acquisition can be handled using pixel-based probabilistic approaches such as particle filters [15], [14], JPDA methods [17], [5], [18], modeling of perceivability [7], target cardinality [19] or iterative and alternative object detection and tracking [4].

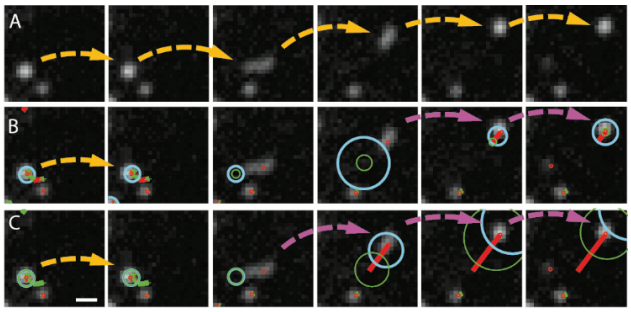

Fig. 1 Challenges in tracking particles undergoing rapid motion type switches. A) After a phase of confined diffusion, the particle displays a fast directed motion before returning to a confined diffusion state. B) An IMM based algorithm cannot not retrieve the directed motion segment; only the Brownian segments are correctly tracked. Small red circles, particle detections. Yellow arrows, true association between detections. Purple arrows, true associations in a secondary trajectory. Red and Green segments, Directed and Brownian motion regime, respectively. Blue and Green circles, search radii estimated at each time point for the Directed and Brownian motion regimes, respectively. C) The u-track algorithm recovers part of the directed motion segment thanks to its Kalman filter initialization routine.

A remaining important challenge in the field is motion heterogeneity in crowded scenes as it arises, for example, with the jerky motion of vesicles and viruses switching between cytoplasmic diffusion and motor-mediated, fast displacements [20]. A non-exhaustive list of such behavior includes axon neurofilament transport by fast motors in an asynchronous fashion [21], virus migration that intermittently exploits endosomal directed transport to reach the nucleus (e.g. HIV [22]), or intermediate filament protein transport along the cytoskeleton as described in [23]. Recent works have focused on the characterization of such trajectories [24]–[27], but none of them discuss the estimation of the trajectory themselves, making the implicit assumptions that the acquisition frequency is high enough to make tracking non-challenging. However, phototoxicity and photobleaching drastically limit the frequency of excitation during live cell imaging. In a dense context, dynamical switches are particularly challenging to

[1]This research has been funded by NIH P01 GM096971, Matisse Graduate School, Inria, France-BioImaging infrastructure supported by the French National Research Agency (ANR-10-INBS-04-07, "Investments for the future"), CPRIT recruitment award R1216, and the UTSW Endowed Scholars Program.

Philippe Roudot (philippe.roudot@utsouthwestern.edu) and Gaudenz Danuser (gaudenz.danuser@utsouthwestern.edu) are with UT Southwestern Medical Center, Lyda Hill Department of Bioinformatics, Dallas, TX 75390 USA. Liya Ding (liyad@alleninstitute.org) is with Allen Institute for Cell Science Seattle, WA 98109, USA. Khuloud Jaqaman (khuloud.jaqaman@utsouthwestern.edu) is with UT Southwestern Medical Center, Department of Biophysics, Dallas, TX 75390 USA. Charles Kervrann (charles.kervrann@inria.fr) is with Inria, Centre de Rennes - Bretagne Atlantique, Serpico Project-Team, Rennes 35000, France.

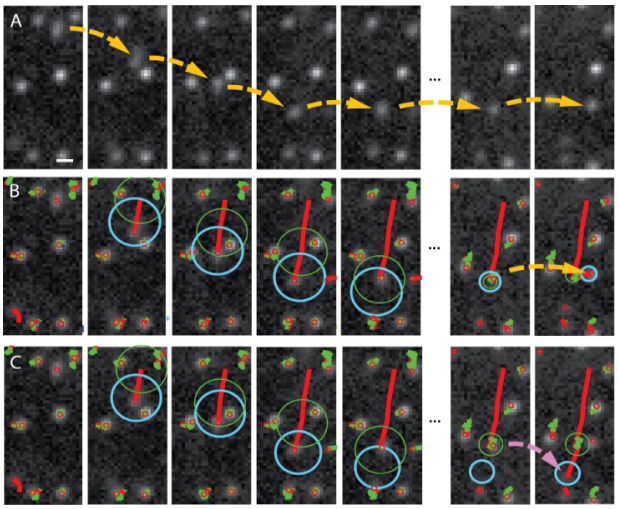

Fig. 2 Challenges in tracking particles with heterogeneous motion in dense condition. A) The particle moves fast and then switches to confined Brownian motion. B) An IMM-based algorithm produces a correct track, switching to a Brownian motion scheme (yellow arrow). C) The u-track algorithm produces a false positive (purple arrow) due to the strong persistence of its directed prediction approach.

detect because they are sudden, unpredictable and also rare in most scenarios. Figures 1 and 2 show two typical cases of those tracking challenges in live cell images. Figure 1A gives an example of a sudden switch from confined diffusion to directed motion. Figure 1B illustrates that an Interacting Multiple Model (IMM) estimator, a state-of-the-art method to model motion heterogeneity (described in Section II.A), cannot predict such a rapid transitions. An obvious solution is to enlarge the search radius, but this is at the cost of increasing the probability of false positives in dense conditions. Figure 1C shows that the u-track method [3] manages to recover a part of the directed motion. This behavior is due to its speed initialization strategy that exploits a tracking pass in the reverse direction (see Section II.A). Figure 2A highlights another challenging scenario where a particle transitions from directed to confined motion in dense particle conditions. IMM allows the correct detection of the Brownian transition (Figure 2B). On the same example, the u-track method produces a false positive due to the strong persistence of its motion predictor (see Section II.A) combined with the spontaneous initiation of a particle trajectory in the immediate neighborhood (Figure 2C). Thus, both IMM and u-track methods suffer limitations in different scenarios.

In this paper, we first review related motion modeling approaches with a focus on their strengths and weaknesses in tracking heterogeneous motions in dense particle fields (Section II). Based on the conclusions from this analysis, we designed a method that combines the flexibility of the IMM-based approach and the robustness of the u-track motion prediction in a novel statistical framework for tracking (Section III). We first describe a piecewise-stationary motion model (PMM) along with an appropriate filtering method. Then, to tackle the unpredictability of switches between types of motion, a piecewise-stationary motion model smoother is considered (PMMS). It exploits recursive tracking in multiple rounds in forward and backward temporal directions to detect stationary motion regimes and smoothen each of the regimes independently. This allows us to predict and recover spontaneous transitions from freely or confined diffusive to directed motion. We also exploit recursive tracking in a temporally and spatially local adaptive estimation of the search radius for assignment (a.k.a. gating). Our approach requires only two frames to associate the set of predictions to the set of measurements while taking into account the information lying in the entire sequence. The algorithm is implemented for 2D data on top of the existing u-track platform and keeps the computational complexity of a deterministic method (10% overhead with respect to u-track). Our new motion model and estimator will part of the next release of the u-track platform at http://www.utsouthwestern.edu/labs/danuser/software/. We show on simulated data that the PMMS algorithm improves the performances of competing heterogeneous motion estimators in different scenarios (Section IV). On the 2D particle tracking challenge datasets presented in [28], a blind execution on the final dataset after parameterization on training datasets shows superior performance of our approach on scenarios with dense particles and competitive results overall. In order to separate as best as possible the problem of motion modeling and object detection, those comparisons have been performed on the high SNR datasets of the challenge. On the vimentin particle experiment illustrated in Figures 1 and 2, we can measure biologically meaningful shifts in the dynamics of very few particles that remained undetectable by other tracking approaches (Section V.A). We also demonstrate that our new method shows better robustness with respect to frame-rate reduction than other multiple model based methods (Section V.B).

II. Related Works

Several reviews on multi-particle tracking (MPT) have been published. Technical descriptions of tracking algorithms have been presented in [2], [29]. Later in [30], a classification and comparison of biological particle and cell tracking software has been introduced. In this section, we review the computational strategies that have been put in place to track heterogeneous motion. For methods on particle modeling and detection the reader is referred to [31]–[34]. Similarly, the combinatorial optimization approaches used to estimate the optimal pairing between a set of predictions and a set of measurements is not discussed in detail in this Section. Advances in this domain, such as multi-frame trackers [7], [8], simulated annealing techniques [11] or batch approaches [12], allow consideration of past and future time points in a fixed temporal window to provide better temporal consistency. However, these algorithms are independent of the motion modeling approaches that assign a cost to each possible track. In practice, the cost associated to each track relies on the standard IMM filtering that uses the past information only [5], [7], [8], [28]. As a result, tracks presenting unpredictable changes of motions type will be assigned a high cost and not selected by the optimization framework. A recent review indicates that the improvements conferred by multi-frame tracking are more impactful under conditions with numerous detection false positives than with motion model complexity [9].

In this section we focus on methods that have been used to model diffusion, directed and heterogeneous transport. We also review strategies to estimate the spatial gating parameter (or search radius), a crucial aspect when dealing with crowded scenes and unpredictable motion transitions.

A. Motion modeling

The most common techniques proposed in the literature to estimate the dynamical parameters of intracellular objects relate to the Kalman filter and its generalization to multiple motion modeling. In this section, we briefly review the Kalman filter to introduce notation and then detail the approximation made in the derivation of the less commonly described multiple motion modeling algorithm. We conclude this section with a brief overview of other motion modeling approaches.

A.1 Kalman filtering

Assuming linear relations in the state space of a particle between consecutive time points and normal-distributed measurement and model noise, it is established that Kalman filtering [35] provides the optimal state estimation. In single particle tracking [36], [37] the vector state of a particle $\mathbf{x}_t$ at time t is often modeled by its position and speed or an equivalent description:

$$\mathbf{x}_t = (x_t, y_t, dx_t, dy_t)^\top. \tag{2.1}$$

The filtering problem can be described as follows:

$$\mathbf{x}_{t+1} = \mathbf{F}\mathbf{x}_t + \mathbf{w}_{t+1} \tag{2.2}$$

$$\mathbf{z}_{t+1} = \mathbf{H}\mathbf{x}_{t+1} + \mathbf{v}_{t+1} \tag{2.3}$$

where the transition matrix $\mathbf{F}$ defines the motion type modeled by the filter, usually expressed as:

$$\mathbf{F} = \begin{pmatrix} 1 & 0 & 0 & 0 \\ 0 & 1 & 0 & 0 \\ 0 & 0 & 0 & 0 \\ 0 & 0 & 0 & 0 \end{pmatrix} \quad \text{and} \quad \mathbf{F} = \begin{pmatrix} 1 & 0 & 1 & 0 \\ 0 & 1 & 0 & 1 \\ 0 & 0 & 1 & 0 \\ 0 & 0 & 0 & 1 \end{pmatrix} \tag{2.4}$$

for Brownian and directed motion, respectively. We used these two transition matrices throughout this work, unless indicated otherwise. The matrix $\mathbf{H}$ is an observation matrix projecting from the state space to the measurement space. The variables $\mathbf{w}_t$ and $\mathbf{v}_t$ represent the model noise and the measurement noise, respectively. Both variables are assumed to represent white noise with covariance matrices $\mathbf{Q}_t$ and $\mathbf{R}_t$. In the framework of Bayesian sequential estimation, the filtering distribution $p(\mathbf{x}_{1:t+1}|\mathbf{z}_{1:t+1}) \sim \mathcal{N}(\hat{\mathbf{x}}_{t+1}, \bar{\mathbf{P}}_{t+1})$ can be computed recursively as derived in [38]. The prediction step yields:

$$\bar{\mathbf{x}}_{t+1} = \mathbf{F}\hat{\mathbf{x}}_t \tag{2.5}$$

$$\bar{\mathbf{P}}_{t+1} = \mathbf{F}\hat{\mathbf{P}}_t\mathbf{F}^\top + \mathbf{Q}_t \tag{2.6}$$

where $\bar{\mathbf{x}}_{t+1}$ and $\bar{\mathbf{P}}_{t+1}$ denote, respectively, the predicted state vector and covariance matrix at time $t+1$. The filtered predictions are used to assign each track with the best matching measurement at $t+1$. The assignment is followed by an update step when a new measurement $\mathbf{z}_{t+1}$ is available:

$$\mathbf{K}_{t+1} = \frac{\bar{\mathbf{P}}_{t+1}\mathbf{H}^\top}{\mathbf{H}\bar{\mathbf{P}}_{t+1}\mathbf{H}^\top + \mathbf{R}_{t+1}} \tag{2.7}$$

$$\hat{\mathbf{P}}_{t+1} = (\mathbf{I} - \mathbf{K}_{t+1}\mathbf{H})\bar{\mathbf{P}}_{t+1} \tag{2.8}$$

$$\hat{\mathbf{x}}_{t+1} = \bar{\mathbf{x}}_{t+1} + \mathbf{K}_{t+1}(\mathbf{z}_{t+1} - \mathbf{H}\bar{\mathbf{x}}_{t+1}) \tag{2.9}$$

where $\mathbf{K}_{t+1}$ is the adaptive Kalman gain applied to the measured innovation $(\mathbf{z}_{t+1} - \mathbf{H}\bar{\mathbf{x}}_{t+1})$ and $\mathbf{I}$ denotes the identity matrix.

A.2 Filtering of multiple motion models

A single Kalman filter cannot take into account the heterogeneity of motion that can be observed in intracellular transport. Moreover, a single constant speed model is not reactive enough to deal with unpredictable changes in the observed motion of a particle [13]. To handle multiple motion types, tracking methods in the radar literature [39], [40], [1] use multiple Kalman Filters with different transition matrices:

$$\mathbf{x}_{t+1} = \mathbf{F}^{\theta_{t+1}}\mathbf{x}_t + \mathbf{w}_{t+1}^{\theta_{t+1}} \tag{2.10}$$

$$\mathbf{z}_{t+1} = \mathbf{H}^{\theta_{t+1}}\mathbf{x}_{t+1} + \mathbf{v}_{t+1}^{\theta_{t+1}}, \tag{2.11}$$

where $\theta_t \in \Lambda = \{1, \ldots, N\}$ and $\theta_{1:t} = \{\theta_1, \theta_2, \ldots, \theta_t\}$ is the unknown sequence of model indices assumed to follow a homogeneous Markov process, and $\mathbf{F}^{\theta_{t+1}}$ is the transition matrix associated to the dynamical model $\theta_{t+1} \in \Lambda$. The same indexed notation applies for the other Kalman filtering variables introduced above. Accordingly, each possible sequence for $\theta_{1:t}$ should be considered to filter the state parameter optimally as:

$$\begin{aligned} p(\mathbf{x}_{t+1}, \mathbf{z}_{1:t+1}) &= \sum_{\theta_2 \in \Lambda} \cdots \sum_{\theta_{t+1} \in \Lambda} p(\mathbf{x}_{t+1}, \mathbf{z}_{1:t+1}, \theta_2, \ldots, \theta_{t+1}) \\ &\propto \sum_{\theta_2 \in \Lambda} \cdots \sum_{\theta_{t+1} \in \Lambda} p(\theta_{2:t+1}|\mathbf{z}_{1:t+1}) p(\mathbf{x}_{t+1}|\mathbf{z}_{1:t+1}, \theta_{2:t+1}) \end{aligned} \tag{2.12}$$

according to the marginalization rule and factorization. The parameter space describing $\theta_{1:t}$ is exponentially increasing with time. This model "history" [1] would thus require an exponentially growing number of Kalman filters to estimate the *a posteriori* distribution of each mode sequence. A common approximation is to consider the possible modes at time $t+1$ [1]:

$$p(\mathbf{x}_{t+1}, \mathbf{z}_{1:t+1}) \propto\!\!\!\sim \sum_{\theta_{t+1} \in \Lambda} p(\theta_{t+1}|\mathbf{z}_{1:t+1}) p(\mathbf{x}_{t+1}|\mathbf{z}_{1:t+1}, \theta_{t+1}) \tag{2.13}$$

where $\propto\!\!\!\sim$ denotes proportionality and approximation. The first term is assumed to follow a Gaussian distribution:

$$p(\mathbf{x}_{t+1}|\mathbf{z}_{1:t+1}, \theta_{t+1}) \sim \mathcal{N}(\hat{\mathbf{x}}_{t+1}^{\theta_{t+1}}, \hat{\mathbf{P}}_{t+1}^{\theta_{t+1}}), \tag{2.14}$$

where $\mathbf{x}_{t+1}^{\theta_{t+1}}$ and $\mathbf{P}_{t+1}^{\theta_{t+1}}$ denote, respectively, the mode conditional mean and the covariance. A Gaussian mixture thus yields the expectation and covariance of the overall posterior at time step $t+1$:

$$\hat{\mathbf{x}}_{t+1} = \sum_{\theta_{t+1} \in \Lambda} p(\theta_{t+1}|\mathbf{z}_{1:t+1}) \hat{\mathbf{x}}_{t+1}^{\theta_{t+1}} \tag{2.15}$$

$$\begin{aligned} \hat{\mathbf{P}}_{t+1} = &\sum_{\theta_{t+1} \in \Lambda} p(\theta_{t+1}|\mathbf{z}_{1:t+1}) \\ &\times \left(\hat{\mathbf{P}}_{t+1}^{\theta_{t+1}} + (\hat{\mathbf{x}}_{t+1}^{\theta_{t+1}} - \hat{\mathbf{x}}_{t+1})(\hat{\mathbf{x}}_{t+1}^{\theta_{t+1}} - \hat{\mathbf{x}}_{t+1})^\top \right). \end{aligned}$$

To compute these moments, the conditional state probability follows the Bayesian filtering rule as:

$$\begin{aligned} &p(\mathbf{x}_{t+1}|\mathbf{z}_{1:t+1}, \theta_{t+1}) \\ &= \frac{p(\mathbf{z}_{t+1}|\mathbf{x}_{t+1}, \theta_{t+1})}{p(\mathbf{z}_{t+1}|\mathbf{z}_{1:t}, \theta_{t+1})} \; p(\mathbf{x}_{t+1}|\mathbf{z}_{1:t}, \theta_{t+1}) \\ &= \frac{p(\mathbf{z}_{t+1}|\mathbf{x}_{t+1}, \theta_{t+1})}{p(\mathbf{z}_{t+1}|\mathbf{z}_{1:t}, \theta_{t+1})} \int p(\mathbf{x}_{t+1}|\mathbf{x}_t, \theta_{t+1}) p(\mathbf{x}_t|\mathbf{z}_{1:t}, \theta_{t+1}) d\mathbf{x}_t. \end{aligned} \tag{2.16}$$

Different implementations of multiple motion models correspond to different choice or modeling of $p(\mathbf{x}_t|\mathbf{z}_{1:t}, \theta_{t+1})$ in order to provide recursive solutions to the estimation of $\mathbf{x}_{t+1}^{\theta_{t+1}}$ and $\mathbf{P}_{t+1}^{\theta_{t+1}}$ in the Kalman filtering framework. The mode probability $p(\theta_t|\mathbf{z}_{1:t}), \forall \theta_t \in \Lambda$, can be derived recursively as:

$$p(\theta_{t+1}|\mathbf{z}_{1:t+1}) \propto p(\mathbf{z}_{t+1}|\mathbf{z}_{1:t}, \theta_{t+1}) \sum_{\theta_t \in \Lambda} p(\theta_{t+1}|\theta_t) p(\theta_t|\mathbf{z}_{1:t}), \quad (2.17)$$

where

$$p(\mathbf{z}_{t+1}|\mathbf{z}_{1:t}, \theta_{t+1}) \sim \mathcal{N}(\mathbf{H}\bar{\mathbf{x}}_{t+1}^{\theta_{t+1}}, \mathbf{H}\bar{\mathbf{P}}_{t+1}^{\theta_{t+1}}\mathbf{H}^\top + \mathbf{R}_t^{\theta_{t+1}}). \quad (2.18)$$

In [3], [13], the authors have introduced different approaches to model motion heterogeneity in bioimaging. The IMM filter borrowed from the radar literature was first applied by [13]. It is well characterized and by now widespread in MPT [7], [11], [19], [30]. The dynamic filtering approaches used in the u-track method [3] has not been described as formally yet. In what follows we interpret it as a Generalized Pseudo Bayesian filter of order 1. After introduction of the framework, we compare the implementation of the u-track algorithm with the more conventional IMM approach.

First-order Generalized Pseudo Bayesian filter (GBP1)

The GBP1 has primarily been described by [41] and is reviewed in [1], [42]. In this modeling approach, the mode at time $t+1$ is assumed to be independent from the state at time t, hence:

$$p(\mathbf{x}_t|\mathbf{z}_{1:t}, \theta_{t+1}) \sim \mathcal{N}(\widehat{\mathbf{x}}_t, \widehat{\mathbf{P}}_t). \quad (2.19)$$

Taking together (2.19) with (2.16) and (2.13), GPB1 performs a recursion between $p(\mathbf{x}_{t+1}|\mathbf{z}_{1:t+1})$ and $p(\mathbf{x}_t|\mathbf{z}_{1:t})$. By identifying (2.16) to the analytical development of a Kalman filter, the mode conditional probability is estimated using the following Kalman filtering equations:

$$\begin{aligned} \bar{\mathbf{x}}_{t+1}^{\theta_{t+1}} &= \mathbf{F}^{\theta_{t+1}}\widehat{\mathbf{x}}_t & \mathbf{K}_{t+1}^{\theta_{t+1}} &= \frac{\bar{\mathbf{P}}_{t+1}^{\theta_{t+1}}\mathbf{H}^\top}{\mathbf{H}\bar{\mathbf{P}}_{t+1}^{\theta_{t+1}}\mathbf{H}^\top + \mathbf{R}_{t+1}} \\ \bar{\mathbf{P}}_{t+1}^{\theta_{t+1}} &= \mathbf{F}^{\theta_{t+1}}\widehat{\mathbf{P}}_t\mathbf{F}^{\theta_{t+1}\top} + \mathbf{Q}_t & \widehat{\mathbf{P}}_{t+1}^{\theta_{t+1}} &= (\mathbf{I} - \mathbf{K}_{t+1}^{\theta_{t+1}}\mathbf{H})\bar{\mathbf{P}}_{t+1}^{\theta_{t+1}} \\ & & \widehat{\mathbf{x}}_{t+1}^{\theta_{t+1}} &= \bar{\mathbf{x}}_{t+1}^{\theta_{t+1}} + \mathbf{K}_{t+1}^{\theta_{t+1}}(\mathbf{z}_{t+1} - \mathbf{H}\bar{\mathbf{x}}_{t+1}^{\theta_{t+1}}) \end{aligned} \quad (2.20)$$

The u-track algorithm [3] reused this principle. In order to handle switches between independent regimes of diffuse and directed motion, a notable difference is the non-mixing of mode-specific conditional estimates, using:

$$\begin{cases} p(\theta_{t+1}|\mathbf{z}_{1:t+1}) = 1 & \text{if} \quad \theta_{t+1} = \underset{\theta_{t+1} \in \Lambda}{\operatorname{argmax}}\ p(\mathbf{z}_{t+1}|\mathbf{z}_{1:t}, \theta_{t+1}) \\ p(\theta_{t+1}|\mathbf{z}_{1:t+1}) = 0 & \text{else} \end{cases} \quad (2.21)$$

Using this approximation, the u-track algorithm can operate N prediction steps with only one set of Kalman filter variables.

Interacting multiple model filter

In the IMM approach [39], a recursive estimation of the model transition probability is exploited to increase the amount of information available from the model "history" while maintaining N competing Kalman filters. This method has been primarily designed for the detection of smooth transitions in aircraft dynamics between cruising (directed displacement) and maneuvering (Brownian model or constant acceleration model). In bioimaging, it was exploited for the first time in [13] to track multiple particles. To model smooth transitions, the conditional probability $p(\mathbf{x}_t|\mathbf{z}_{1:t}, \theta_{t+1})$ is further linked to the previous mode according to the marginalization rule:

$$p(\mathbf{x}_t|\mathbf{z}_{1:t}, \theta_{t+1}) \propto \sum_{\theta_t \in \Lambda} p(\mathbf{x}_t|\mathbf{z}_{1:t}, \theta_t) p(\theta_t|\theta_{t+1}, \mathbf{z}_{1:t}), \quad (2.22)$$

where the approximation (2.14) also applies at time t. Accordingly, given $\theta_{t+1} \in \Lambda$, the conditional state probability at time t is as follows:

$$p(\mathbf{x}_t|\mathbf{z}_{1:t}, \theta_t) \sim \mathcal{N}(\widehat{\mathbf{x}}_t^{\theta_t}, \widehat{\mathbf{P}}_t^{\theta_t}), \quad (2.23)$$

and

$$p(\mathbf{x}_t|\mathbf{z}_{1:t}, \theta_{t+1}) \sim \mathcal{N}(\tilde{\mathbf{x}}_t^{\theta_{t+1}}, \tilde{\mathbf{P}}_t^{\theta_{t+1}}) \quad (2.24)$$

with the "mixing" of estimates:

$$\tilde{\mathbf{x}}_t^{\theta_{t+1}} = \sum_{\theta_t \in \Lambda} p(\theta_t|\theta_{t+1}, \mathbf{z}_{1:t}) \widehat{\mathbf{x}}_t^{\theta_t} \quad (2.25)$$

$$\tilde{\mathbf{P}}_t^{\theta_{t+1}} = \sum_{\theta_t \in \Lambda} p(\theta_t|\theta_{t+1}, \mathbf{z}_{1:t}) \left(\widehat{\mathbf{P}}_t^{\theta_t} + (\widehat{\mathbf{x}}_t^{\theta_t} - \tilde{\mathbf{x}}_t^{\theta_{t+1}})(\widehat{\mathbf{x}}_t^{\theta_t} - \tilde{\mathbf{x}}_t^{\theta_{t+1}})^\top \right).$$

The equation (2.16) can thus again be interpreted as a prediction followed by a sensor update in a Kalman filter. As a result, for each mode $\theta_{t+1} \in \Lambda$, an estimation cycle is defined as:

$$\begin{aligned} \bar{\mathbf{x}}_{t+1}^{\theta_{t+1}} &= \mathbf{F}^{\theta_{t+1}}\tilde{\mathbf{x}}_t^{\theta_{t+1}} & \mathbf{K}_{t+1}^{\theta_{t+1}} &= \frac{\bar{\mathbf{P}}_{t+1}^{\theta_{t+1}}\mathbf{H}^\top}{\mathbf{H}\bar{\mathbf{P}}_{t+1}^{\theta_{t+1}}\mathbf{H}^\top + \mathbf{R}_{t+1}} \\ \bar{\mathbf{P}}_{t+1}^{\theta_{t+1}} &= \mathbf{F}^{\theta_{t+1}}\tilde{\mathbf{P}}_t^{\theta_{t+1}}\mathbf{F}^{\theta_{t+1}\top} + \mathbf{Q}_t & \widehat{\mathbf{P}}_{t+1}^{\theta_{t+1}} &= (\mathbf{I} - \mathbf{K}_{t+1}^{\theta_{t+1}}\mathbf{H})\bar{\mathbf{P}}_{t+1}^{\theta_{t+1}} \\ & & \widehat{\mathbf{x}}_{t+1}^{\theta_{t+1}} &= \bar{\mathbf{x}}_{t+1}^{\theta_{t+1}} + \mathbf{K}_{t+1}^{\theta_{t+1}}(\mathbf{z}_{t+1} - \mathbf{H}\bar{\mathbf{x}}_{t+1}^{\theta_{t+1}}) \end{aligned} \quad (2.26)$$

The "mixing" of the input variable at the beginning of the cycle is controlled by the estimated transition probabilities:

$$\begin{aligned} p(\theta_t|\theta_{t+1}, \mathbf{z}_{1:t}) &\propto p(\theta_{t+1}|\theta_t, \mathbf{z}_{1:t}) p(\theta_t|\mathbf{z}_{1:t}), \\ &= p(\theta_{t+1}|\theta_t) p(\theta_t|\mathbf{z}_{1:t}). \end{aligned} \quad (2.27)$$

The probability $p(\theta_t|\mathbf{z}_{1:t}), \forall \theta_t \in \Lambda$ is computed recursively following (2.17). By design, an IMM estimator always balances the contributions of all Kalman Filters. Implicitly, this yields smoothness in the transition between motion models.

Implementations of multiple modeling algorithms

The differences between the algorithms proposed in [13] and [3] reside in theory and implementation. A combination of three aspects must be taken into account to understand the differences highlighted in Figures 1 and 2. The first aspect is the state initialization. To initialize speed, u-track performs three rounds of tracking in forward and backward directions by reversing the temporal order of the image sequence. A second aspect of u-track is the transition matrix used to model the Brownian state:

$$\mathbf{F} = \begin{pmatrix} 1 & 0 & 0 & 0 \\ 0 & 1 & 0 & 0 \\ 0 & 0 & 1 & 0 \\ 0 & 0 & 0 & 1 \end{pmatrix} \quad (2.28)$$

This model results in a complete transmission of the speed vector $(dx_t, dy_t)^\top$ in the filtered estimation of the state parameter by the Brownian Kalman filter as far as the estimated

gain is low. A third aspect is that u-track maintains a single state estimate, following the GPB1 principle. As a result, if a particle stays in a Brownian state and follows this model, a low innovation will be measured and the temporal filter will leave the speed estimate unfiltered.

The consequence of this implementation is that the speed component of the estimates $\hat{\mathrm{x}}_t$ can converge to a single vector $(\widehat{dx}_t, \widehat{dy}_t)^\top$ during the three rounds of tracking, provided that the directed regimes captured by the forward and backward runs are similar in direction and speed and even if multiple motion type switches occur between directed and Brownian displacement. This increases robustness in the detection of directed displacements intercepting Brownian walks. For example, Figure 1C illustrates the ability of the u-track algorithm to predict and capture part of the directed regime; this is due to the conservation of the directed speed estimate during forward and backward tracking. On the same data, a more classical IMM is only able to recover the Brownian segments. Figure 2 highlights the limitations arising with this approach. The inertia of the GPB1 filter and the unique speed estimation result in false positives in dense and heterogeneous conditions. In our new tracking method, we will combine the two approaches to benefit from IMM's flexibility and the efficient convergence properties of u-track.

A.3 Other related approaches

Particle filtering approaches have also been proposed in MPT [43]. The exponential complexity due to the simultaneous tracking of several objects combined with the tendency of the particle filter to coalesce on a single mode can be problematic if the object number of particles is large [14]. To circumvent this issue, mixture of particles [14] and independent particle filters [15], have been proposed. Nevertheless, as particle filter based methods present a high computational cost and the objects (spots) look very similar [15], these probabilistic approaches are often applied in sparse and noisy scenario [14], [15]. One example of motion heterogeneity modeling can be found in [44] where particle filtering is used to estimate ``stop-and-go" dynamics of growing axons.

In [45], the authors proposed a greedy approach to quantifying directed axonal transport without Bayesian filtering. Given a set of tracks at time t each possible trajectory up to time $t + \Delta$ is built (Δ is set to six in the experiment). The "cost" of each possible track is then computed based on speed, intensity and track length as a weighting cue. Contrary to filter-based methods, this estimator exploits past and future measurements in its cost estimate and thus could potentially handle unpredictable switching with an ad hoc piecewise cost function. However, this approach is computationally prohibitive when applied to the whole sequence. To alleviate this problem, the authors proposed to reduce the temporal window, which in turn reduced the number of sample used to estimate the motion parameter at each time point.

Finally, a large collection of other methods model motion as stationary Brownian using a global covariance parameter to model diffusive behavior (see [4], [6], [11], [46], [47]).

A.4 Discussion

The flexibility and simplicity of multiple motion model filtering in the Kalman framework offers the best trade-off between heterogeneous motion modeling and computational cost. This theoretical argument has been confirmed in practical applications of the algorithm in the ISBI 2012 MPT challenge [28]. However, filtering techniques only make use of the motion history of the particles. Accordingly, those methods cannot predict sudden changes of direction. In the method described in this paper, we propose a piecewise-stationary motion model to take into account instantaneous dynamical change. To be able to forecast these rapid changes in motion regime while keeping a computationally efficient per-track basis, we exploit past and future measurements in the sequence with a stochastic smoothing approach.

B. Spatial gating

The spatial gating parameter is useful to lower computational cost, and required to handle track initiation and termination. In a crowded scene, heterogeneous behavior calls for an adaptive search radius estimation framework to avoid false positive links caused by misdetections of track terminations. Most methods rely on a global covariance parameter either set manually by the user [4], [6], [15], trained offline by simulations [12], or estimated globally using the average estimation errors across all tracks [11]. In [13], [3], the authors proposed a per-track adaptive approach by using the covariance of the innovation and the covariance matrix of the prediction error in the measurement space. In [3], the covariance matrix is estimated using:

$$\hat{\mathbf{S}}_t = \mathrm{Var}[\mathbf{K}_t\,(\mathbf{z}_t - \mathbf{H}\mathbf{x}_t)]_{1:t} \tag{2.29}$$

The search radius is then based on its projection on the observable space, using a p-value applied to the normal distribution described by the innovation covariance matrix and the current state estimate [13], or an equivalent heuristic [3]:

$$\mathbf{C}_t = \lambda(2\mathbf{H}^t\hat{\mathbf{S}}_t\mathbf{H})^{\frac{1}{2}} \tag{2.30}$$

As we show in the following experiments, we can improve these techniques by proposing a search radius estimator that adapts to fast switching between different dynamical regimes.

III. OUR METHOD

Rapid changes in type of transport or motion model parameters combined with a high particle density can severely hinder the reconstruction of complete trajectories. Our strategies to overcome those issues are twofold: stochastic smoothing and piecewise-stationary motion modeling.

Because a stochastic filter only accounts for the past, numerous motion variations, such as a switch from Brownian to rapid directed movement or fast to slow motion, cannot be predicted. This frequently leads to early track termination as illustrated by Figure 1. On the other hand, such a transition may be much more predictable in the reverse temporal order. In order to fuse both perspectives, we propose a stochastic smoothing approach to multiple motion modeling in the form of a two-filter smoother. We also exploit our smoother to adjust the search radius using a frame-by-frame iterative approach. As a result each particle displacement is predicted by considering past and future measurements without the need for a time window larger than two time points.

An additional problem for particle tracking in live cell imaging originates in the uncorrelated nature of different motion regimes within one trajectory. Oftentimes, the switches from motor-mediated motion to local jiggling or Brownian diffusion and back are triggered by biochemical reactions that occur suddenly at the time scale of image sampling. IMM as much as GBP1 methods have been primarily designed to detect maneuver of aircraft with transitions over multiple time points [40]. In the IMM algorithm this "soft switching" [1] is modeled by "mixing" [40] the Kalman filter estimates of the different modes in order to recondition the overall posterior (see equations 2.25 and 2.27). This is incompatible with fast switches. Here, we replace the smooth transition model with a piecewise-stationary motion model : Each motion regime in the sequence of measurement is smoothed independently using a piecewise-stationary motion model smoother that performs three tracking rounds in forward - reverse – forward order (see Figure 3). Transitions between regimes are detected on-the-fly and handled by adaptive reinitialization of Kalman filtering variables.

We implemented the PMMS algorithm on top of the u-track platform for three reasons: i) the modular design of u-track supports implementation of multiple strategies for dynamic filtering; ii) u-track provides an optimized linear programming solution for pairwise association of prediction and measurement; this makes tracking suitable in scenarios in which the particle density is too high for computationally efficient comparison of multiple hypothetical tracks over multiple frames; iii) contrary to multi-frame MHT approaches, the gap closing step is separated from the frame-to-frame linking. Instead interrupted track segments are connected in a second optimization step, which implicitly takes into account past and future information while keeping low computational cost. Hence, we could restrict the implementation of the PMMS to the frame-to-frame linking step and make use of the existing gap closing approach. The approach does not add any user-defined control parameters to the original u-track method. As with the original platform, the frame-to-frame linking step requires the definition of allowable motion models (Brownian and directed motion models are implemented already, but more can be added), the parameter λ from equation (2.30), an initial guess of the search radius C_t in the first iteration of tracking and an optional lower and upper bound for the automatic adaptation of the search radius. The gap closing step requires a definition of the maximum gap time and the minimum length for tracks to be considered for gap closing, in addition to the above-mentioned parameters for the search radius definition.

Following we first introduce the PMM and its consequence on the derivation of the piecewise-stationary motion model filter (Sections III.A and III.B). We then introduce our two-filter iterative smoother in Section III.C and describe our on-line estimation of the search radius in each track in Section III.D.

A. Motion modeling

Unpredictable switches in a Markov chain break the assumption of white Gaussian process noise in the Kalman filter. This problem has been first tackled by Kitagawa [48], who proposed

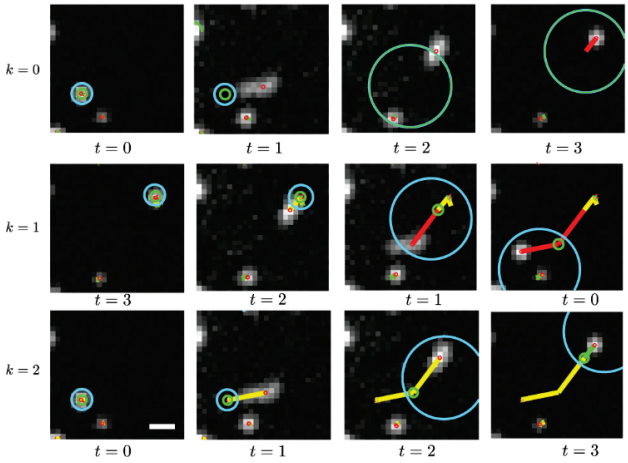

Fig. 3 Our iterative smoothing approach on an example. Red links represent directed prediction selection, green link represent Brownian prediction and yellow represent predictions that coincide with the previous tracking round. A small displacement is easily retrieved during the first tracking round, it serves as a track initialization for the following track rounds.

a new estimator that explicitly estimates a non-Gaussian posterior distribution in a Bayesian framework that preceded the particle filtering approaches. Those approaches require computationally costly parameterization of the non-Gaussian distribution. In the PMM, we describe each of the stationary motion regimes with the following state predictor and measurement models:

$$\mathbf{x}_{t+1} = \mathbf{F}^{\theta_i}\mathbf{x}_t + \mathbf{w}_{t+1}^{\theta_i} \tag{3.1}$$

$$\mathbf{z}_{t+1} = \mathbf{H}^{\theta_i}\mathbf{x}_{t+1} + \mathbf{v}_{t+1}^{\theta_i}, \tag{3.2}$$

using the same notation as in Section II.A. Here, $\theta_i \in \Lambda$ with $i \in \{0, \aleph - 1\}$ represent successive stationary regimes with time points $\mathrm{T} = \{T_0, \ldots, T_\aleph\}$ marking the beginnings and ends of the regimes.

B. Piecewise-stationary motion model filtering

Using our model, equation (2.13) is no longer an approximation. Instead we write:

$$\begin{aligned} p(\mathbf{x}_{t+1}, \mathbf{z}_{1:t+1}) &= p(\mathbf{x}_{t+1}, \mathbf{z}_{T_i:t+1}) \\ &\propto \sum_{\theta_i \in \Lambda} p(\mathbf{x}_{t+1}|\mathbf{z}_{T_i:t+1}, \theta_i) p(\theta_i|\mathbf{z}_{T_i:t+1}) \end{aligned} \tag{3.3}$$

where T_i is the start time of the current motion regime. The conditional state probability then derives from a classic multiple model filter as well, i.e.,

$$\begin{aligned} &p(\mathbf{x}_{t+1}|\mathbf{z}_{T_i:t+1}, \theta_i) \\ &= \frac{p(\mathbf{z}_{t+1}|\mathbf{x}_{t+1}, \theta_i)}{p(\mathbf{z}_{t+1}|\mathbf{z}_{T_i:t}, \theta_i)}\, p(\mathbf{x}_{t+1}|\mathbf{z}_{T_i:t}, \theta_i) \\ &= \frac{p(\mathbf{z}_{t+1}|\mathbf{x}_{t+1}, \theta_i)}{p(\mathbf{z}_{t+1}|\mathbf{z}_{T_i:t}, \theta_i)} \int p(\mathbf{x}_{t+1}|\mathbf{x}_t, \theta_i) p(\mathbf{x}_t|\mathbf{z}_{T_i:t}, \theta_i) d\mathbf{x}_t. \end{aligned} \tag{3.4}$$

Using the same Gaussian assumption described in Section II, this equation is equivalent to a Kalman filter prediction and update. However, an important difference is that each Kalman filter associated to a motion regime iterates on its own without variable mixing between regimes. This mechanism has been dubbed as 'static multiple modeling' in [1], yet without the

piecewise-stationary framework proposed here. We reproduce below the associated filtering cycle:

$$\begin{aligned}
\bar{\mathbf{x}}_{t+1}^{\theta_i} &= \mathbf{F}^{\theta_i}\hat{\mathbf{x}}_t^{\theta_i} & \mathbf{K}_{t+1}^{\theta_i} &= \frac{\bar{\mathbf{P}}_{t+1}^{\theta_i}\mathbf{H}^{\theta_i\top}}{\mathbf{H}^{\theta_i}\bar{\mathbf{P}}_{t+1}^{\theta_i}\mathbf{H}^{\theta_i\top}+\mathbf{R}_{t+1}} \\
\mathbf{P}_{t+1}^{\theta_i} &= \mathbf{F}^{\theta_i}\hat{\mathbf{P}}_t^{\theta_i}\mathbf{F}^{\theta_i\top}+\mathbf{Q}_t^{\theta_i} & \widehat{\mathbf{P}}_{t+1}^{\theta_i} &= (\mathbf{I}-\mathbf{K}_{t+1}^{\theta_i}\mathbf{H}^{\theta_i})\bar{\mathbf{P}}_{t+1}^{\theta_i} \\
& & \widehat{\mathbf{x}}_{t+1}^{\theta_i} &= \bar{\mathbf{x}}_{t+1}^{\theta_i}+\mathbf{K}_{t+1}^{\theta_i}(\mathbf{z}_{t+1}-\mathbf{H}^{\theta_i}\bar{\mathbf{x}}_{t+1}^{\theta_i})
\end{aligned} \tag{3.5}$$

for $\theta_i \in \Lambda$. The mode probability also derives from (2.17):

$$p(\theta_i|\mathbf{z}_{T_i:t+1}) \propto p(\mathbf{z}_{t+1}|\mathbf{z}_{T_i:t},\theta_i)p(\theta_i|\mathbf{z}_{T_i:t}) \tag{3.6}$$

with the conditional probability of the new measurement defined similarly as in Section II.A. In the filtering approach, we detect changes in the transport mode on-the-fly by testing if the new measurement contradicts the stationarity assumption. Hence, we have $t+1 \in \mathrm{T}$ if:

$$\underset{\theta_i\in\Lambda}{\operatorname{argmax}}\ p(\mathbf{z}_{t+1}|\mathbf{z}_{T_i:t},\theta_i) \neq \underset{\theta_i\in\Lambda}{\operatorname{argmax}}\ p(\theta_i|\mathbf{z}_{T_i:t}) \tag{3.7}$$

Finally, this same assumption of stationarity yields

$$\widehat{\mathbf{x}}_t = \widehat{\mathbf{x}}_t^{\hat{\theta}_i} \quad \text{and} \quad \widehat{\mathbf{P}}_t = \widehat{\mathbf{P}}_t^{\hat{\theta}_i} \tag{3.8}$$

with $\hat{\theta}_i$ denoting the most likely motion mode. Upon detection of a new motion regime, all Kalman filters are re-initialized using the estimate yielded by the last filtering cycle. Because the estimation relates to the previous motion regime, this initialization is clearly suboptimal, especially in the case of large and sudden apparent changes in the dynamics of the particle. The smoothing approach described in the following section addresses this issue.

C. *Two-filter piecewise-stationary motion smoothing*

To improve the detection of switching from one motion regime to another, the concept of smoothing comes as a natural way of exploiting past and future measurements to maximize the amount of information at hand. In conventional MPT methods, the rationale for filtering is not to obtain the best estimates associated to each measurement in a known trajectory. The objective is to provide the optimization scheme with the most accurate prediction to select the optimal link among multiple candidates. Accordingly, widespread correcting smoothers such as the Rauch-Tung-Striebel framework [49] are not suitable as they only use a backward pass to refine the estimates carried out for each measurement in a first forward filtering pass. We thus propose the application of an approach introduced in the 1960s by Fraser and Potter [50], referred to as a two-filter smoother. The smoother fuses two independent Kalman filtering processes carried out in forward and backward temporal order. In the Bayesian framework, it follows as:

$$\begin{aligned}
p(\mathbf{x}_{t+1}|\mathbf{z}_{1:T_\aleph}) &= p(\mathbf{x}_{t+1}|\mathbf{z}_{T_i:T_{i+1}}) \\
&\propto p(\mathbf{x}_{t+1}|\mathbf{z}_{T_i:t})p(\mathbf{z}_{t+1:T_{i+1}}|\mathbf{x}_{t+1}).
\end{aligned} \tag{3.9}$$

A non-trivial probabilistic derivation has been proposed in [51], [52], demonstrating that the estimates of the variable describing $p(\mathbf{x}_t|\mathbf{z}_{1:T}) \sim \mathcal{N}(\widehat{\mathbf{x}}_t, \widehat{\mathbf{P}}_t)$ are given by:

$$\widehat{\mathbf{x}}_t = \widehat{\mathbf{P}}_t\left(\widehat{\mathbf{P}}_t^{f^{-1}}\widehat{\mathbf{x}}_t^f + \widehat{\mathbf{P}}_t^{b^{-1}}\widehat{\mathbf{x}}_t^b\right) \tag{3.10}$$

$$\widehat{\mathbf{P}}_t = \left(\widehat{\mathbf{P}}_t^{f^{-1}} + \widehat{\mathbf{P}}_t^{b^{-1}}\right)^{-1} \tag{3.11}$$

where the indices *f* and *b* indicate forward and reverse piecewise filtering, respectively. Contrary to a correcting smoother, this provides us with two independent predictions for each time point.

In order to build the transition time set T, the mode stationarity is tested for each time point using the same condition as in (3.7). In this section, we denote the resulting transition time set with T_{θ_i}. Additionally, we test if both forward and reverse filters converge on the same mode using:

$$\underset{\theta_i\in\Lambda}{\operatorname{argmax}}\ p(\mathbf{z}_{t+1}|\mathbf{z}_{T_i:t},\theta_i) = \underset{\theta_i\in\Lambda}{\operatorname{argmax}}\ p(\mathbf{z}_t|\mathbf{z}_{t+1:T_{i+1}},\theta_i). \tag{3.12}$$

Each time point that does not fulfill this condition is considered a boundary between two independent motion regimes, constituting the set $\mathrm{T}_{\theta_i'}$. In a MPT context, the optimal measurement at each time point must also be selected. The solution is straightforward when both filters select the same sequence of measurement such as

$$\begin{aligned}
\mathbf{z}_{t+1} &= \underset{\mathbf{z}\in D_{t+1}}{\operatorname{argmax}}\ p(\mathbf{z}|\mathbf{z}_{T_i:t},\hat{\theta}_i^f) \\
\mathbf{z}_t &= \underset{\mathbf{z}\in D_t}{\operatorname{argmax}}\ p(\mathbf{z}|\mathbf{z}_{t+1:T_{i+1}},\hat{\theta}_i^b),
\end{aligned} \tag{3.13}$$

where D_{t+1} is the set of particle detections in time point *t*+1. If this condition is not fulfilled, we propose to select the new measurement with the highest likelihood. Additionally, we define the time point $t+1$ as a boundary of a motion regime collected in the time set $\mathrm{T}_{\mathbf{z}}$. Indeed even though two consecutive modes can be the same, the selection of two different measurements justifies the definition of two independent motion regimes. When no measurement is selected by either one of the two filters, we set its state covariance matrix to infinity. In parallel to the estimation of the transition time set $\mathrm{T} = \mathrm{T}_{\theta_i} \cup \mathrm{T}_{\theta_i'} \cup \mathrm{T}_{\mathbf{z}}$ each regime must be smoothed independently. In the following we propose an iterative framework to carry out both estimations.

In our implementation of the PMMS, we arbitrarily choose to start with forward filtering. This first step allows the construction of T_{θ_i} along the first filtering process. A backward filter will test each newly estimated time point building $\mathrm{T}_{\theta_i'}$ and $\mathrm{T}_{\mathbf{z}}$. For each time point $T_i \in \mathrm{T}$, the backward filter must be reinitialized using $\mathbf{x}_{T_i}^b = \mathbf{x}_{T_i}^f$ to reflect the shift in motion. To complete the smoothing of each regime, the forward filtering must be carried out again considering the entire set of transition times in T. More formally, let us define the tracking round $k+1$ as the reverse to a preceding forward tracking round *k*, with $k=0$ referring to the first forward round. With $\hat{\theta}_{i,k}$ denoting the most likely motion mode at tracking round *k*, we define

$$\widehat{\mathbf{x}}_{t,k+1}^{\hat{\theta}_{i,k+1}} = \widehat{\mathbf{P}}_{t,k+1}^{\hat{\theta}_{i,k+1}}\left(\widehat{\mathbf{P}}_t^{\hat{\theta}_i^{-1}}\widehat{\mathbf{x}}_t^{\hat{\theta}_i} + \widehat{\mathbf{P}}_{t,k}^{\hat{\theta}_{i,k}^{-1}}\widehat{\mathbf{x}}_{t,k}^{\hat{\theta}_{i,k}}\right) \tag{3.14}$$

$$\widehat{\mathbf{P}}_{t,k+1}^{\hat{\theta}_{i,k+1}} = \left(\widehat{\mathbf{P}}_t^{\hat{\theta}_i^{-1}} + \widehat{\mathbf{P}}_{t,k}^{\hat{\theta}_{i,k}^{-1}}\right)^{-1}. \tag{3.15}$$

Here, the state and covariance $(\hat{\mathbf{x}}_t^{\hat{\theta}_i}, \widehat{\mathbf{P}}_t^{\hat{\theta}_i})$ are computed using the piecewise-stationary motion model filter described in Section III.A with:

$$\mathbf{x}_t^{\theta_i} = \left(\mathbf{F}^{\theta_i}\right)^{(-1)^{k+1}} \hat{\mathbf{x}}_{t+(-1)^k}^{\theta_i} \tag{3.16}$$
$$\bar{\mathbf{P}}_t^{\theta_i} = \left(\mathbf{F}^{\theta_i}\right)^{(-1)^{k+1}} \hat{\mathbf{P}}_{t+(-1)^k}^{\theta_i} \left(\mathbf{F}^{\theta_i}\right)^{(-1)^{k+1}\top} + \mathbf{Q}_{t+(-1)^k}^{\theta_i}.$$

In this smoothing framework, changes in the motion mode and conflict in the measurement selection are detected online at each Kalman filtering prediction step. Every time a change in the motion type is detected the filters are re-initialized using

$$\widehat{\mathbf{x}}_{T_i,k+1}^{\hat{\theta}_{i,k+1}} = \widehat{\mathbf{x}}_{T_i,k}^{\hat{\theta}_{i,k}} \quad \text{and} \quad \widehat{\mathbf{P}}_{T_i,k+1}^{\hat{\theta}_{i,k+1}} = \widehat{\mathbf{P}}_{T_i,k}^{\hat{\theta}_{i,k}}. \tag{3.17}$$

Each independent Kalman filter is thus properly initialized with a value trained on a measurement sequence associated with the corresponding regime, i.e.,

$$p(\mathbf{x}_{T_{i+1}}^b) = p(\mathbf{x}_{T_{i+1}}^f | \mathbf{z}_{T_i:T_{i+1}}) \tag{3.18}$$
$$p(\mathbf{x}_{T_i}^f) = p(\mathbf{x}_{T_i}^b | \mathbf{z}_{T_i:T_{i+1}}).$$

An important advantage of the PMMS is its reliance on a cost-effective two-frame-based optimization scheme that accounts for the information contained in the entire time sequence. Naturally, this approach is compatible with a multi-frame MHT approach.

D. Online Iterative gating parameter estimation

We exploit the iterative aspect of our algorithm to robustly estimate the spatial component of the covariance matrix of the prediction error for each motion regime. Based on this estimate, we propose an adaptive estimation of the search radius to handle unpredictable changes.

First, we save memory by adapting the classic online variance estimator to our problem. At each time step, the parameter triplet $(m_{t,k}, n_{t,k}, M_{t,k})$ is updated for the most probable mode:

$$\bar{\delta}_{t+1} = \mathbf{K}_{t+1}^{\hat{\theta}_{i,k}}(\mathbf{z}_{t+1} - \mathbf{H}\mathbf{x}_{t+1,k}^{\hat{\theta}_{i,k}}) \tag{3.19}$$
$$n_{t+1,k}^{\hat{\theta}_i} = n_{t,k}^{\hat{\theta}_i} + 1$$
$$m_{t+1,k}^{\hat{\theta}_i} = m_{t,k}^{\hat{\theta}_i} + \frac{\bar{\delta}_{t+1} - m_{t,k}^{\hat{\theta}_i}}{n_{t+1,k}^{\hat{\theta}_i}}$$
$$M_{t+1,k}^{\hat{\theta}_i} = M_{t,k}^{\hat{\theta}_i} + (\bar{\delta}_{t+1} - m_{t+1,k}^{\hat{\theta}_i})^\top (\bar{\delta}_{t+1} - m_{t+1,k}^{\hat{\theta}_i}),$$

where $n_{t+1,k} \in \mathbb{N}$ is the count of prediction errors, $m_{t+1,k} \in \mathbb{R}$ is the associated mean and $M_{t+1,k} \in \mathbb{R}$ is the sum of squares of differences from the mean. The covariance matrix is thus estimated as

$$\hat{\mathbf{S}}_{t+1,k} = \frac{M_{t+1,k}}{n_{t+1,k}} \tag{3.20}$$

and the search radius follows then from (2.30). This method can only converge towards a single covariance estimation for the whole track, which is insufficient with heterogeneous motion. Most notably, the transition from directed to Brownian motion can trigger a substantial overestimation of the search radius. Our algorithm thus reinitializes the covariance depending on the motion regime transition. In the first iteration of filtering, a parameter set $(m_{t,k}^0, n_{t,k}^0, M_{t,k}^0)$ dedicated to Brownian motion is maintained for each track. When a motion type switch from directed to Brownian displacement is detected (condition (3.7)) the triplet $(m_{t,k}, n_{t,k}, M_{t,k})$ is reset to $(m_{t,k}^0, n_{t,k}^0, M_{t,k}^0)$. Similarly to Section III.C, we then exploit the iterative properties of our algorithm to refine the initialization of each regime. If the time-point t is part of $\mathbb{T}$ we use the noise estimation variable from the previous tracking round:

$$(m_{t,k+1}, n_{t,k+1}, M_{t,k+1}) = (m_{t,k}, n_{t,k}, M_{t,k}). \tag{3.21}$$

We thus obtain a prediction error estimate adapted to each motion regime in a track. Figure 4 shows a simplified overview of our algorithm. The flowchart highlights the piecewise filtering process and iterative tracking.

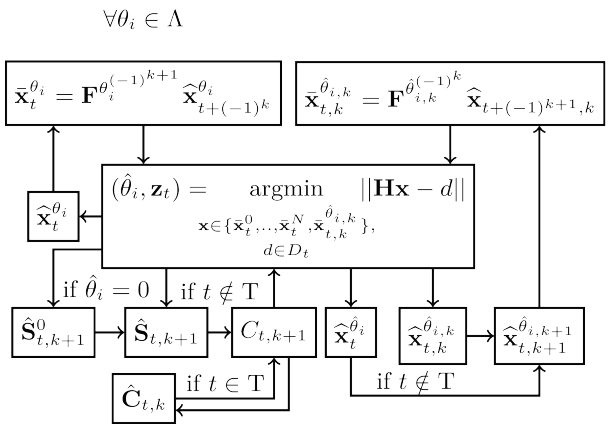

Fig. 4 Overview of tracking algorithm at round k+1. For the sake of clarity, covariance matrix and Kalman filter variable updates are not indicated.

IV. Results on simulated data

In this section, we focus the analysis of the performances of the PMMS on simulated data. We first demonstrate the performance of our algorithm with respect to our targeted problem, i.e. the tracking of vesicles with high density and motion heterogeneity. We show that it behaves advantageously over other tracking approaches. We then also show that our algorithm can outperform other approaches in more homogeneous scenarios. Finally, we test the performance of our approach on the MPT datasets proposed in [28].

A. Heterogeneity and density of particles

In order to evaluate the motion modeling performance, our simulation framework tests only for the accuracy of the estimated trajectories and not the particle detection. The simulated motion is controlled by two parameters: motion heterogeneity and particle density. Heterogeneity is modeled by the probability of having a motion type switch between confined Brownian and directed motion at a given time point. With a simulated acquisition frame-rate of 1 frame/s, every simulated track starts with confined Brownian motion with a 2D diffusion coefficient uniformly distributed from 0.025 to 6.25 $\mu m^2/s$ (0.01 to 16 pixels^2/frame) and a confinement area with the same distribution from 0.0625 to 3 $\mu m^2/s$ (0.25 to 4

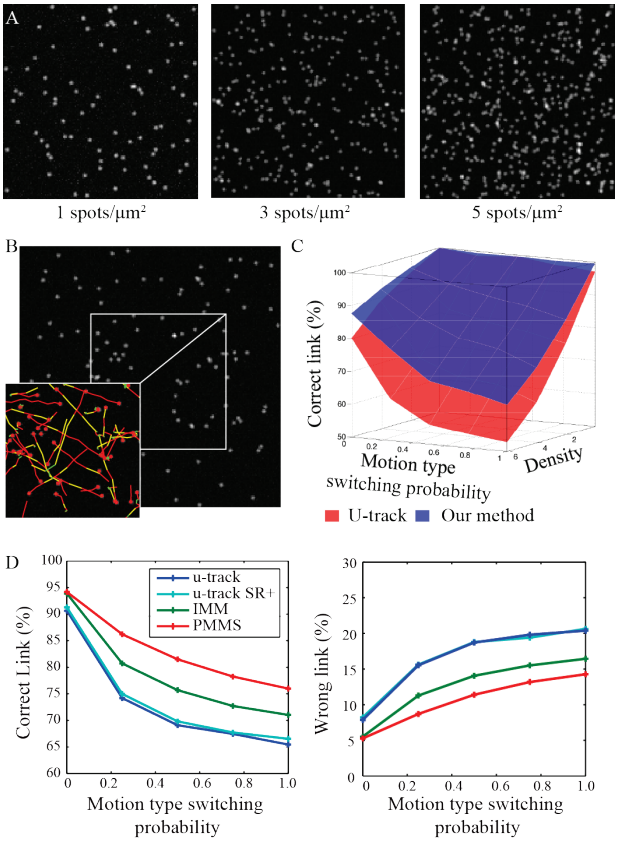

Fig. 5 A) Range of simulated particle density. B) Example of simulated tracks with a particle density of 1 spots/μm^2 (red (resp. yellow) segment: better likelihood with the current (resp. previous inverted) filtering round). C) Percentage of correct links as a function of density and motion type switching probability. Our method outperforms u-track by 15% in the most difficult case. D) True positive and false positive ratio on the same simulation with a density of 3 spots/μm^2 comparing our method with u-track, u-track with an online process noise estimator and an IMM algorithm with forward-backward initialization.

pixels^2/frame). The directed segment speed follows a uniform random distribution bounded by 0.5 $\mu m/s$ (10 pixels/frame) in a 10 μm by 10 μm image (200×200 pixels). The direction is chosen randomly for each directed segment and stays constant with an additional Brownian component simulated as described above. The track length follows the same normal probability distribution with mean 50 s and a standard deviation of 20 s for every simulation and each sequence is 500 frames long. To test the effect of density, we tune the number of particles from 1 to 6 spots/ μm^2 (a 20x20 pixel square). Figure 5A illustrates the rendering of particles with a density of 1 to 5 spots/ μm^2. Figure 5B displays simulated particle motion in a field with 1 spots/ μm^2density.

We compared the PMMS with the original u-track algorithm, the same algorithm augmented with a recursive gating parameter estimation (u-track SR+) allowing for a better search radius estimation on short tracks and an IMM algorithm similar to the work in [13]. For a fair test, we implemented the IMM algorithm in the u-track framework with combinatorial optimization [53] and a forward-backward tracking scheme for Kalman filter initialization. Figure 5C presents the impact of both density and heterogeneity on the tracking performances of the original u-track and the new method. The percentage of correct and wrong links is computed relative to the number of simulated links. Clearly, the new approach is superior in every

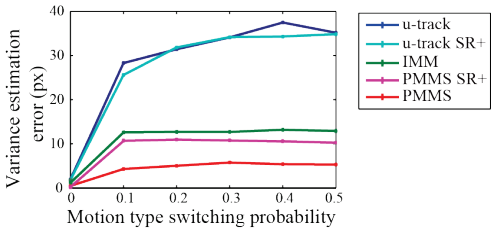

Fig. 6 Error in the estimation of the covariance matrix of the innovation as a function of the motion switching probability. Simulated data is used. Vesicle density is set to 3 spots/μm^2. Our method is compared with the estimation of the covariance matrix of the innovation on the whole track up to time t (u-track) and an online and iterative though non adaptive variance estimation (u-track SR+).

aspect. The comparison reveals a stronger impact of motion heterogeneity on performance difference with an increase of 10% to 25% in correct linking count when the chance to undergo a change in motion regime at each time point is set to one. Performances also increase with density, with a measured improvement from 2 to 25% in the highest density scenario. Figure 5D provides a more complete overview of the performances with respect to motion heterogeneity, using a fixed density of 3 spots/ μm^2. This data shows the different performances of the GPB1 algorithm and the IMM as well as the added value of the PMMS. Our approach more than doubles the performance gain provided by our implementation of IMM with respect to u-track when motion heterogeneity is high. The superiority of our method increases with motion switch probability. Given the very similar performance of u-track and u-track SR+ (less than 0.5 difference in performances), we omit the results from this method in the following for the sake of clarity.

Using a simulated density of 3 spots/ μm^2 (a 20x20 pixel square) and an heterogeneity of 0.5 in a 10 μm by 10 μm image (200×200 pixels) over 500 frames, the linking and gap closing part of the original u-track algorithm takes 194 s on a standard workstation using a single 3.5 GHz processor with 32Gb of RAM. The computational overhead of our PMMS is only 10% more in the worst case compared to u-track and is similar to our implementation of IMM.

B. Gating parameter

We assessed independently the performance of our adaptive gating parameter estimator using the same simulations in Figure 5D. Figure 6 indicates that the error in the estimation of the simulated model noise is reduced when using our adaptive approach instead of a conventional variance estimate (see Section II.B). To compare the performances between our adaptive approach and u-track in a fair manner, the u-track SR+ augment the algorithm with an online estimator for the covariance matrix of the prediction error that exploits the forward-backward initialization process of u-track to initialize the covariance matrix at the beginning of each track. One can note that this addition alone has little impact. We also implemented the same online estimation on the IMM method and PMMS approach (named respectively IMM and PMMS SR+) considering the prediction error of the most probable mode at each time point without taking advantage of the recursive aspect or handling regime transitions. The performance of both approaches are similar, measuring an estimation error that is twice the error measured with the complete PMMS approach and three times less than the original u-track platform. This shows that our approach, which

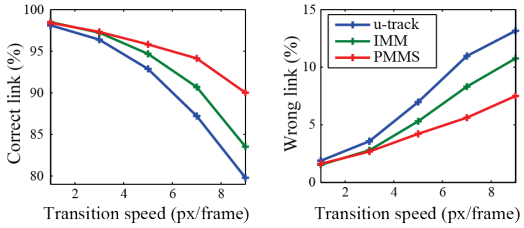

Fig 7. Correct linking and false positive percentage function of the transition speed, density is set to 3 spots/μm^2.

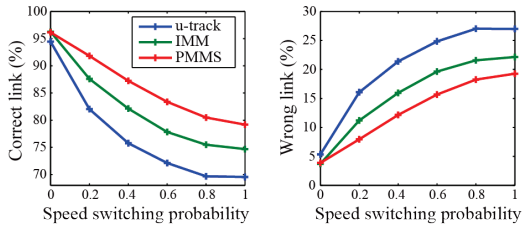

Fig. 8. Correct linking and false positive percentage with respect to speed switching probability.

explicitly accounts for transitions between motion regimes, improves the covariance computation and with it the definition of gating parameters.

C. *Transition speed*

Another interesting parameter in addition to density and heterogeneity is the speed involved in the transition between two motion types. To test for the robustness of our tracker with respect to that parameter we tuned the speed of motor mediated displacement from 0.025 $\mu m/s$ to 0,425 $\mu m/s$ (1.5 to 8.5 pixel/frame) that occur after a long period of confined displacement (Figure 7). Also with respect to this aspect, the PMMS significantly outperforms u-track and the IMM algorithm.

D. *Speed variation*

We also tested the PMMS in the case of stationary directed motion with significant variation in particle speed. In this scenario, there is no switching between Brownian and directed displacement. This mimics, for instance, a scenario where intracellular clutter locally congests vesicle transport with the result that particle motion even within one regime is not constant. In order to test this scenario, we simulated trajectories presenting strictly directed motion but varying speed magnitude. We modeled dynamical instability by tuning the probability of having a speed change at a given time point. At each speed change, the new velocity is drawn from a uniform distribution taking values between 0.05 and 0.5 $\mu m/s$ (1 to 10 pixels/frame) and the density is set to 3 spots/μm^2. In those sequences our method outperforms u-track by 10% (Figure 8), showing its versatility.

E. *Multiple particle tracking challenge data*

A common limitation in the comparison of algorithms is that the test data sets are often designed to highlight the innovation a particular method over the others. To standardize performance analysis in the field of MPT a challenge was set up in 2012 [28]. Among the four test scenarios, three are adequate benchmarks for our contribution: the 'receptor scenario' characterized by heterogeneous motion switching between Brownian and directed motion, the 'vesicle scenario' characterized by free diffusion and the 'microtubule scenario' simulated with directed displacement and comet-shaped particles. Each scenario is simulated with varying particle density: 100, 500 and 1000 particles. To compare the performances of our contribution on motion modeling and estimation, we evaluate the PMMS on the simulated SNR 4 and 7 that are challenged by dynamical complexity in a dense environment rather than detection sensitivity. Let us note that, in the scenario 'receptor' and 'microtubule', the speed is simulated as stationary and equal for all trajectories making transition between motion regimes less challenging than in the simulations described previously.

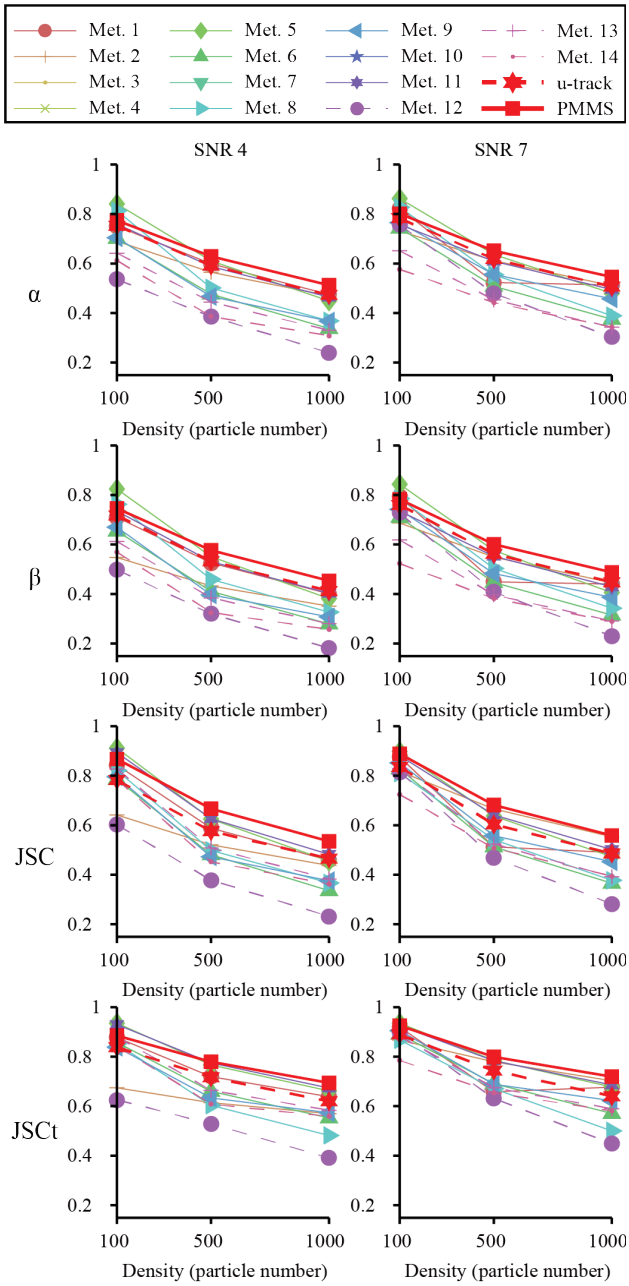

Fig. 9 Average performances measured on the Vesicle dataset (Brownian diffusion), Microtubule dataset (directed displacement) and Receptor scenario (heterogeneous displacement) datasets provided in the MPT challenge (see text for definition of metrics).

Tracking performances were assessed based on the following metrics: **α** is the overall distance between the estimated set of trajectories and the ground truth without considering false positives (1 is perfect match), the Jaccard Similarity Coefficient (JSC) is the detection rate in the estimated track set (1 is all particle belong to a track without false positive), **β** is the overall track distance balanced by the number of spurious tracks (**β=α** when there is no spurious tracks), and the Jaccard Similarity Coefficient applied to tracks (JSCt) is the rate of correct tracks, with a tracks being considered valid if a majority of points correspond to a true track (1 is a perfect match). Fourteen teams have taken part in the challenge. After algorithm parameterization with the training data sets, each method was tested on the final challenge dataset. While no single method stood out clearly, the organizers concluded that multi-frame techniques such as MHT and motion modeling such as IMM-based techniques are more likely to perform better.

We use the detector described in our previous work in [54]. For each pixel, the local background and amplitude of a Gaussian function with fixed position and scale is estimated. A threshold of significance is then computed from the fitting residuals. Each significant pixel that co-localizes with a local maximum in the Laplacian-of-Gaussian filtered original image subsequently is fitted with a Gaussian particle intensity model to define the centroid position of a particle. In the case of the microtubule scenario, an additional step estimates the comet orientation using an anisotropic Gaussian fitting. The comet intensity is integrated along the major half-axis of the ellipsoidal support. The local maximum of the resulting intensity profile is selected as the comet position along the comet axis. In order to match the original conditions of the challenge, we tuned the control parameters of our algorithm on the training data before a blind execution on the final challenge data. Figure 9 shows the evaluation of the average performance on both scenarios on the four tracking-related metric as a function of the particle density.

Although our implementation of PMMS does not employ multi-frame optimization for particle assignment, it exhibited the best performance on average in this challenge dataset at the highest and medium density for both tested SNR and among the top 4 for the sparsest case. This underscores the advantages of the approach in crowded particle fields even with relatively homogeneous motion behavior. The same set of parameters were used for each scenario, SNR and density conditions, showing the self-adaptation of the proposed PMMS. The microtubule scenario did not employ the Brownian Kalman filter.

Table 1 compares the PMMS performances (Orange and yellow background highlight best and second best score) to the methods that reached the top 2 in at least one of the performance metrics in at least one of simulations in the challenge. As expected, the PMMS performs particularly well on the ‘receptor scenario’, it ranks first or second in medium and high density on all metrics except in the JSCt measure of the case SNR 4 at medium density where it is a close third. Our approach is also very competitive in the ‘vesicle scenario’, ranking in first, second or third position in the highest density. In the low density benchmark, the methods 3, 4, 5 and 7 outperform our implementation in separate scenarios. Methods 3, 4 and 7 use a multi-frame optimization framework that is inherently more robust against detection false negatives [30] while method 5 refines trajectories by fusing the Kalman filtering prediction and detection to refine localization. Method 3 is absent from Table 1a because of the lack of microtubule results submitted to the challenge. With respect to the ’vesicle’ and ‘receptor’ scenarios, our method performs better than Method 3 on average in the highest density (data not shown). Of note, the PMMS motion model and estimation framework is complementary to these approaches in that it augments the cost function for track assignment. It is thus very likely that

TABLE. 1
OVERVIEW OF OUR PERFORMANCE IN THE MPT CHALLENGE.

Metric	α						β						JSC						JSCt					
SNR	4			7			4			7			4			7			4			7		
Density	low	med	high	low	med	high	low	med	high	low	med	high	low	med	high	low	med	high	low	med	high	low	med	high
Met. 1	0.75	0.6	0.48	0.82	0.52	0.51	0.71	0.53	0.4	0.79	0.45	0.44	0.84	0.59	0.46	0.88	0.51	0.49	0.88	0.72	0.64	0.92	0.66	0.68
Met. 2	0.69	0.56	0.47	0.73	0.61	0.51	0.55	0.43	0.35	0.69	0.55	0.45	0.64	0.52	0.44	0.82	0.67	0.55	0.67	0.61	0.57	0.87	0.78	0.7
Met. 5	0.84	0.61	0.45	0.86	0.64	0.48	0.82	0.55	0.38	0.84	0.58	0.41	0.91	0.63	0.46	0.9	0.64	0.47	0.93	0.77	0.66	0.93	0.78	0.68
Met. 8	0.81	0.5	0.37	0.83	0.55	0.39	0.76	0.46	0.33	0.79	0.5	0.34	0.82	0.5	0.37	0.81	0.54	0.38	0.85	0.6	0.48	0.87	0.67	0.5
Met. 11	0.76	0.59	0.46	0.76	0.61	0.5	0.73	0.53	0.4	0.73	0.55	0.43	0.89	0.63	0.48	0.88	0.64	0.5	0.93	0.77	0.67	0.92	0.78	0.69
Met. 13	0.64	0.44	0.33	0.65	0.45	0.34	0.61	0.38	0.28	0.62	0.4	0.29	0.83	0.51	0.38	0.83	0.52	0.39	0.88	0.66	0.58	0.88	0.67	0.59
u-track	0.75	0.59	0.47	0.78	0.62	0.51	0.72	0.53	0.41	0.76	0.56	0.45	0.78	0.58	0.47	0.84	0.6	0.49	0.84	0.72	0.62	0.89	0.74	0.64
PMMS	0.77	0.63	0.51	0.8	0.65	0.55	0.75	0.58	0.45	0.78	0.6	0.49	0.87	0.67	0.54	0.89	0.68	0.56	0.88	0.78	0.69	0.92	0.8	0.72

a) Average performances

Metric	α						β						JSC						JSCt					
SNR	4			7			4			7			4			7			4			7		
Density	low	med	high	low	med	high	low	med	high	low	med	high	low	med	high	low	med	high	low	med	high	low	med	high
Met. 1	0.91	0.76	0.62	0.92	0.47	0.66	0.9	0.7	0.55	0.91	0.4	0.59	0.94	0.74	0.59	0.92	0.44	0.62	0.96	0.84	0.73	0.95	0.57	0.76
Met. 3	0.9	0.79	0.67	0.89	0.79	0.69	0.9	0.76	0.62	0.87	0.75	0.65	0.98	0.84	0.69	0.95	0.82	0.72	0.98	0.89	0.81	0.96	0.9	0.82
Met. 5	0.89	0.71	0.55	0.91	0.72	0.56	0.88	0.66	0.47	0.89	0.67	0.49	0.94	0.71	0.53	0.92	0.71	0.54	0.96	0.83	0.71	0.95	0.83	0.72
Met. 11	0.92	0.77	0.64	0.93	0.79	0.67	0.91	0.73	0.58	0.91	0.74	0.61	0.96	0.76	0.63	0.93	0.77	0.64	0.96	0.87	0.76	0.95	0.86	0.78
u-track	0.86	0.77	0.67	0.89	0.79	0.71	0.84	0.72	0.61	0.87	0.74	0.65	0.81	0.71	0.6	0.83	0.73	0.62	0.88	0.82	0.71	0.92	0.82	0.72
PMMS	0.86	0.78	0.68	0.91	0.81	0.72	0.84	0.74	0.62	0.9	0.76	0.67	0.89	0.78	0.67	0.92	0.79	0.69	0.92	0.86	0.78	0.95	0.86	0.8

b) Receptor scenario

Metric	α						β						JSC						JSCt					
SNR	4			7			4			7			4			7			4			7		
Density	low	med	high	low	med	high	low	med	high	low	med	high	low	med	high	low	med	high	low	med	high	low	med	high
Met. 1	0.8	0.69	0.53	0.89	0.7	0.58	0.73	0.61	0.44	0.85	0.62	0.49	0.79	0.65	0.49	0.87	0.65	0.53	0.79	0.77	0.64	0.91	0.76	0.68
Met. 3	0.84	0.67	0.51	0.84	0.68	0.49	0.82	0.61	0.43	0.81	0.62	0.38	0.91	0.67	0.49	0.88	0.67	0.43	0.92	0.81	0.69	0.94	0.81	0.57
Met. 5	0.88	0.66	0.49	0.88	0.68	0.53	0.86	0.59	0.41	0.85	0.6	0.45	0.92	0.64	0.47	0.88	0.65	0.5	0.93	0.78	0.67	0.92	0.78	0.7
Met. 7	0.67	0.56	0.44	0.67	0.57	0.48	0.65	0.51	0.38	0.66	0.52	0.42	0.92	0.72	0.54	0.92	0.72	0.59	0.93	0.87	0.74	0.98	0.88	0.79
Met. 8	0.81	0.69	0.48	0.88	0.69	0.53	0.73	0.62	0.42	0.84	0.62	0.46	0.77	0.65	0.46	0.86	0.64	0.49	0.79	0.79	0.62	0.91	0.79	0.65
Met. 9	0.81	0.56	0.44	0.82	0.6	0.49	0.78	0.47	0.36	0.8	0.5	0.4	0.88	0.54	0.42	0.88	0.55	0.46	0.81	0.61	0.56	0.92	0.62	0.59
Met. 11	0.85	0.62	0.44	0.86	0.64	0.48	0.81	0.54	0.36	0.84	0.56	0.4	0.85	0.58	0.4	0.86	0.59	0.42	0.91	0.77	0.65	0.93	0.79	0.67
Met. 12	0.68	0.54	0.3	0.86	0.6	0.37	0.66	0.46	0.23	0.84	0.54	0.28	0.72	0.51	0.28	0.87	0.57	0.33	0.66	0.68	0.45	0.94	0.75	0.52
u-track	0.85	0.65	0.49	0.85	0.66	0.53	0.82	0.58	0.41	0.82	0.59	0.46	0.82	0.58	0.46	0.83	0.58	0.48	0.85	0.72	0.6	0.86	0.73	0.62
PMMS	0.86	0.67	0.51	0.86	0.68	0.55	0.83	0.6	0.44	0.83	0.61	0.48	0.88	0.64	0.48	0.85	0.64	0.51	0.9	0.77	0.67	0.89	0.78	0.69

c) Vesicle scenario

Metric	α						β						JSC						JSCt					
SNR	4			7			4			7			4			7			4			7		
Density	low	med	high	low	med	high	low	med	high	low	med	high	low	med	high	low	med	high	low	med	high	low	med	high
Met. 2	0.56	0.47	0.4	0.69	0.56	0.47	0.26	0.23	0.19	0.69	0.54	0.43	0.37	0.34	0.31	0.95	0.76	0.63	0.36	0.36	0.36	0.96	0.85	0.75
Met. 4	0.78	0.56	0.44	0.85	0.64	0.5	0.73	0.51	0.39	0.83	0.6	0.45	0.86	0.61	0.48	0.93	0.69	0.54	0.84	0.73	0.66	0.95	0.8	0.71
Met. 5	0.75	0.46	0.31	0.8	0.51	0.34	0.73	0.4	0.26	0.79	0.45	0.28	0.87	0.52	0.37	0.89	0.56	0.38	0.92	0.7	0.6	0.94	0.74	0.61
Met. 8	0.76	0.15	0.07	0.69	0.27	0.06	0.72	0.14	0.06	0.64	0.22	0.04	0.82	0.19	0.09	0.69	0.28	0.07	0.89	0.23	0.12	0.76	0.39	0.13
Met. 11	0.51	0.38	0.32	0.48	0.41	0.34	0.49	0.32	0.27	0.46	0.35	0.28	0.87	0.54	0.42	0.86	0.57	0.44	0.91	0.69	0.6	0.9	0.7	0.62
u-track	0.55	0.36	0.26	0.61	0.4	0.28	0.5	0.3	0.21	0.59	0.35	0.23	0.72	0.44	0.34	0.84	0.51	0.36	0.78	0.61	0.55	0.89	0.68	0.58
PMMS	0.6	0.44	0.35	0.63	0.47	0.36	0.57	0.39	0.3	0.62	0.42	0.32	0.83	0.58	0.46	0.89	0.62	0.48	0.84	0.7	0.63	0.93	0.75	0.66

d) Microtubule scenario

Orange and yellow background highlight best and second best score.

combining methods would afford even better performances across the spectrum of densities.

V. RESULTS ON EXPERIMENTAL DATA

Our algorithm is primarily designed to track heterogeneous motion behaviors of intra-cellular objects that cannot be recovered by state-of-the-art algorithms. In this section we present quantifications of the motion of vimentin particles and viruses that undergo jerky movements because of their continuous association and dissociation with different classes of molecular motors. Using a virus image data set, we also show the robustness of the PMMS against frame rate reduction, which can be an important asset for the tracking of weakly labeled fluorescent targets and for the reduction of photo-toxicity in general.

A. Vimentin is bound to microtubules

Based on perturbation experiments and end point readouts of the changes in vimentin filament architecture, current models in the literature hypothesize that vimentin particles are transported along the actin and microtubule networks [55]. Visual inspection of live cell movies, however, challenge this

view. The vast majority of vimentin particles seems to undergo tethered Brownian motion without a significant directed component. Very occasionally, it is possible to find an episode of extremely fast motion of an individual particle. Such episodes are observable both in control cells and in cells treated with the drug nocodazole, which induces microtubule disassembly. To test whether microtubule-mediated transport indeed plays a role in vimentin particle transport, it is thus necessary to test differences in the frequency of occurrence of these rare events. Under the current null hypothesis control cells should exhibit significantly more fast motion episodes than cells treated with nocodazole. Live cell fluorescence imaging of GFP-labelled vimentin particles in SW13 cells has been carried out with a spinning disk confocal microscope using a 100x objective (0.16 µm/pixel) at 1 Hz. Eight cells were treated with nocodazole (10 μM), while 12 cells were used as control. Each cell was imaged for two minutes before photobleaching prevented further observation. An average of twenty thousand trajectories per cell was measured in acquisitions presenting up to a hundred thousand displacements in total and of an average of a thousand vimentin particles per frame. We define the threshold for fast motion as the 99.9th percentile of the speed measured on control data i.e. 0.9 µm/s. As shown by Figure 10, the PMMS allows to quantify a small difference between fast motions in control and treated cells in accordance with preliminary studies performed manually [23] and with better statistical significance than the u-track method.

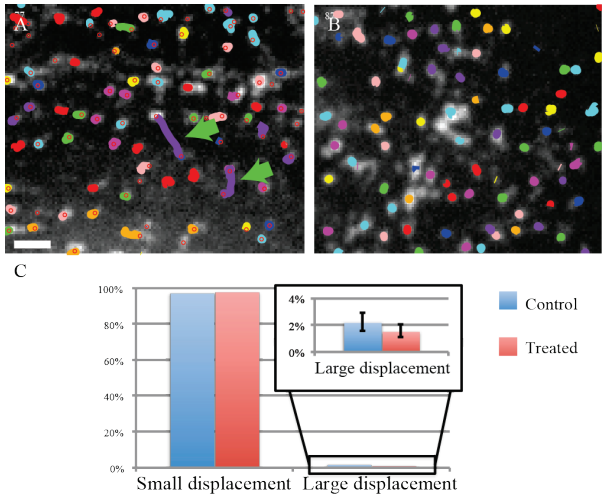

Fig. 10 Vimentin particle movements tracked by the PMMS algorithm. A) Control cell; occasional fast movements are highlighted with green arrows (scale bar is 1 μm). B) Cell after nocodazole treatment; nearly all fast movements are eliminated. C) A threshold for defining large movements is estimated using the 99.9 percentile of the estimated speed distribution. A t-test on 8 cells for each conditions gives a p-value of 0.0088 suggesting that nocodazole treatment effectively hinders fast movements.

B. Robustness against acquisition speed reduction

Particle tracker robustness against low frame-rate is a key aspect in biological imaging as it allows for a reduction of excitation light. We tested this aspect on a published data set of intracellular virus motion [56][57]. In these publications, virus particles were tracked by the method described in [24] using multiple fluorescent labels per virus that allowed an acquisition frequency of 30 Hz. Given the relatively sparse density, motion estimation is not challenging in the original data. Hence, we obtained a ground truth that was amenable to artificial temporal subsampling for the purpose of testing the robustness of the new tracker. Figure 11 illustrates that u-track break point is around a thirty-fold sample decimation while the PMMS estimates the same set of trajectories up to a fifty-fold decimation. To avoid bias toward our new approach, the ground truth was generated using the original u-track platform. Measuring the number of correct tracks versus sample decimation factor, Figure 12 shows that the PMMS performance reduces linearly while the performances of the u-track and IMM method drop quadratically with a reduction of the frame rate. In accordance with our results on simulated data, the performance of the IMM motion modelling approach is roughly half way between the u-track and the PMMS approach. Finally, we performed the same numerical experiment using the method published in [7] and implemented in the ICY platform [58]. The method implements a multi-frame MHT algorithm allowing for short gap closing that also models object detectability to increase robustness in lower SNR scenario. In order to account for implementation and parameterization differences, the decrease in performance is measured relative to the ground truth generated with the MHT method itself. For fairness, we use the same set of detections for the four methods compared. The best performing

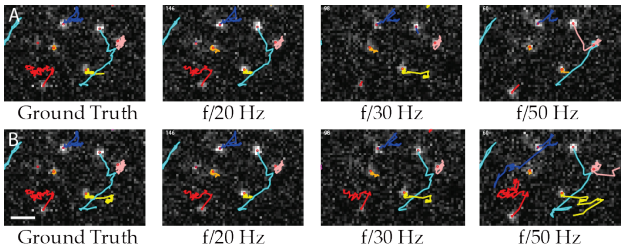

Fig. 11 Virus tracking inside the cell. Frame-rate is artificially reduced to test tracker robustness. A) Tracking results using the u-track method. B) Tracking results using the PMMS algorithm (scale bar is 1 μm. Longer tracks are due to lower frame rate and drag tails plotting but represent real tracks).

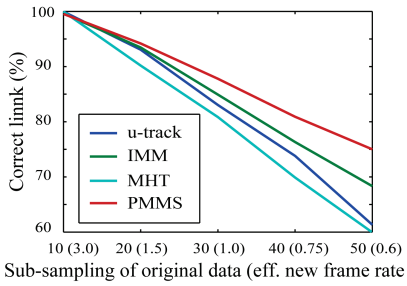

Fig. 12 Percentage of correct link measured by the original u-track compared to IMM, a multi-frame MHT approach (Chenouard *et al* 2013) and our method with respect to frame-rate decimation factor.

set of parameters for the MHT approach is found when disabling adaptive search radius, enabling multiple motion modeling, and using an expected search radius of 6 pixels, a temporal window of 4, an expected track length of 250 frames and a single expected new appearance per frame. We found that the MHT approach performance decreases linearly and at a higher rate than our implementation of the IMM and the PMMS motion models. Provided that the IMM we implemented is similar to the one described in [7], those results could be explained by differences in other strategies such as the use of the recursive tracking for Kalman filter variable initialization. This data also suggest that the use of multiple frame may not be

advantageous in a scenario of limited frame rate and growing unpredictability in motion types.

VI. CONCLUSION

In this work, we have carried out an in-depth review of the multiple motion model estimators described in the literature for the purpose of handling heterogeneous transport in living cells. Based on this analysis, we propose a piecewise-stationary motion model and a new estimator that exploits multiple tracking rounds within an iterative multiple model smoother (PMMS). Our approach allows the estimation of unpredictable switches in the displacement of particles that a propagating filter cannot forecast with linear time complexity. We also proposed a new adaptive search radius to improve gating of possible assignments and better detect terminations in a cluttered environment. The PMMS algorithm has been tested on simulations and is shown to outperform multiple model estimators in heterogeneous conditions. Simulations also show that our method outperforms those methods in scenarios with one motion regime but varying velocity. In an unbiased evaluation on the dataset challenged by dynamical complexity in a dense environment published in [28], our results on high SNR data demonstrate that the PMMS is very competitive, especially in the highest density where it provides the best results on average on the Brownian (Vesicle scenario), directed (microtubule scenario) and heterogeneous (receptor scenario) displacements. On experimental sequences, we show that our method identifies very small but meaningful differences in the heterogeneous dynamics of particles. We also show how the enhanced motion modeling of the PMMS confers robustness against variation in acquisition frame-rate on images capturing heterogeneous virus particle movements. Together these results indicate that the PMMS is a potent solution to the problem of heterogeneous motion tracking of crowded particle fields, which has been a notorious obstacle to high-fidelity analysis of object dynamics, especially in bioimaging applications.

ACKNOWLEDGMENTS

We thank Christoph Burckhardt and Urs Greber from the Institute of Molecular Life Science, University of Zurich, Switzerland, for the adenovirus images.

REFERENCE

[1] Y. Bar-Shalom, X. R. Li, and T. Kirubarajan, *Estimation with applications to tracking and navigation: theory algorithms and software*. John Wiley & Sons, 2001.

[2] Y. Kalaidzidis, “Multiple objects tracking in fluorescence microscopy,” *J. Math. Biol.*, vol. 58, no. 1–2, pp. 57–80, 2009.

[3] K. Jaqaman *et al.*, “Robust single-particle tracking in live-cell time-lapse sequences,” *Nat. Methods*, vol. 5, no. 8, pp. 695–702, 2008.

[4] A. Sergé, N. Bertaux, H. Rigneault, and D. Marguet, “Dynamic multiple-target tracing to probe spatiotemporal cartography of cell membranes,” *Nat. Methods*, vol. 5, no. 8, pp. 687–694, 2008.

[5] W. J. Godinez and K. Rohr, “Tracking Multiple Particles in Fluorescence Time-Lapse Microscopy Images via Probabilistic Data Association,” *IEEE Trans. Med. Imaging*, vol. 34, no. 2, pp. 415–432, Feb. 2015.

[6] I. F. Sbalzarini and P. Koumoutsakos, “Feature point tracking and trajectory analysis for video imaging in cell biology,” *J. Struct. Biol.*, vol. 151, no. 2, pp. 182–195, 2005.

[7] N. Chenouard, I. Bloch, and J. C. Olivo-Marin, “Multiple Hypothesis Tracking for Cluttered Biological Image Sequences,” *IEEE Trans. Pattern Anal. Mach. Intell.*, vol. 35, no. 11, pp. 2736–3750, Nov. 2013.

[8] L. Liang, H. Shen, P. De Camilli, and J. S. Duncan, “A Novel Multiple Hypothesis Based Particle Tracking Method for Clathrin Mediated Endocytosis Analysis Using Fluorescence Microscopy,” *IEEE Trans. Image Process.*, vol. 23, no. 4, pp. 1844–1857, Apr. 2014.

[9] I. Smal and E. Meijering, “Quantitative comparison of multiframe data association techniques for particle tracking in time-lapse fluorescence microscopy,” *Med. Image Anal.*, vol. 24, no. 1, pp. 163–189, Aug. 2015.

[10] A. Jaiswal, W. J. Godinez, R. Eils, M. J. Lehmann, and K. Rohr, “Tracking Virus Particles in Fluorescence Microscopy Images Using Multi-Scale Detection and Multi-Frame Association,” *IEEE Trans. Image Process.*, vol. 24, no. 11, pp. 4122–4136, Nov. 2015.

[11] V. Racine, A. Hertzog, J. Jouanneau, J. Salamero, C. Kervrann, and J.-B. Sibarita, “Multiple-target tracking of 3D fluorescent objects based on simulated annealing,” in *Proc. Int. Symp. on Biomedical Imaging (ISBI)*, Arlington, U.S.A., 2006, pp. 1020–1023.

[12] K. E. G. Magnusson and J. Jalden, “Tracking of non-brownian particles using the Viterbi algorithm,” in *Proc. Int. Symp. on Biomedical Imaging (ISBI)*, New-York, U.S.A., 2015, pp. 380–384.

[13] A. Genovesio, T. Liedl, V. Emiliani, W. J. Parak, M. Coppey-Moisan, and J.-C. Olivo-Marin, “Multiple particle tracking in 3-D+ t microscopy: method and application to the tracking of endocytosed quantum dots,” *IEEE Trans. Image Process.*, vol. 15, no. 5, pp. 1062–1070, 2006.

[14] I. Smal, K. Draegestein, N. Galjart, W. Niessen, and E. Meijering, “Particle filtering for multiple object tracking in dynamic fluorescence microscopy images: Application to microtubule growth analysis,” *IEEE Trans. Med. Imaging*, vol. 27, no. 6, pp. 789–804, 2008.

[15] W. J. Godinez, M. Lampe, S. Wörz, B. Müller, R. Eils, and K. Rohr, “Deterministic and probabilistic approaches for tracking virus particles in time-lapse fluorescence microscopy image sequences,” *Med. Image Anal.*, vol. 13, no. 2, pp. 325–342, 2009.

[16] L. Feng, Y. Xu, Y. Yang, and X. Zheng, “Multiple dense particle tracking in fluorescence microscopy images based on multidimensional assignment,” *J. Struct. Biol.*, vol. 173, no. 2, pp. 219–228, 2011.

[17] S. H. Rezatofighi, S. Gould, R. Hartley, K. Mele, and W. E. Hughes, “Application of the IMM-JPDA filter to multiple target tracking in total internal reflection fluorescence microscopy images,” in *Medical Image Computing and Computer-Assisted Intervention (MICCAI)*, Nice, France: Springer, 2012, pp. 357–364.

[18] I. Smal, W. Niessen, and E. Meijering, “A new detection scheme for multiple object tracking in fluorescence microscopy by joint probabilistic data association filtering,” in *Proc. Int. Symp. on Biomedical Imaging (ISBI)*, Paris, France, 2008, pp. 264–267.

[19] S. H. Rezatofighi, S. Gould, B. T. Vo, B.-N. Vo, K. Mele, and R. Hartley, “Multi-Target Tracking With Time-Varying Clutter Rate and Detection Profile: Application to Time-Lapse Cell Microscopy Sequences,” *IEEE Trans. Med. Imaging*, vol. 34, no. 6, pp. 1336–1348, Jun. 2015.

[20] M. J. Saxton, “Single-particle tracking: models of directed transport,” *Biophys. J.*, vol. 67, no. 5, pp. 2110–2119, 1994.

[21] Y. Li, P. Jung, and A. Brown, “Axonal transport of neurofilaments: a single population of intermittently moving polymers,” *J. Neurosci.*, vol. 32, no. 2, pp. 746–758, 2012.

[22] T. Lagache, E. Dauty, and D. Holcman, “Physical principles and models describing intracellular virus particle dynamics,” *Curr. Opin. Microbiol.*, vol. 12, no. 4, pp. 439–445, 2009.

[23] V. Prahlad, M. Yoon, R. D. Moir, R. D. Vale, and R. D. Goldman, “Rapid movements of vimentin on microtubule tracks: kinesin-dependent assembly of intermediate filament networks,” *J. Cell Biol.*, vol. 143, no. 1, pp. 159–170, 1998.

[24] J. A. Helmuth, C. J. Burckhardt, P. Koumoutsakos, U. F. Greber, and I. F. Sbalzarini, “A novel supervised trajectory segmentation algorithm identifies distinct types of human adenovirus motion in host cells,” *J. Struct. Biol.*, vol. 159, no. 3, pp. 347–358, Sep. 2007.

[25] N. Chenouard and R. W. Tsien, “An algorithm for piecewise-constant velocity estimation and application to particle trajectories in microscopy,” in *Proc. Int. Symp. on Biomedical Imaging (ISBI)*, New-York, U.S.A., 2015, pp. 399–402.

[26] W. J. Godinez, K. Lymperopoulos, D.-P. Herten, and K. Rohr, “Motion analysis of receptors and ligands in high resolution fluorescence microscopy images,” in *Proc. Int. Symp. on Biomedical Imaging (ISBI)*, New-York, U.S.A., 2015, pp. 703–706.

[27] V. Briane, M. Vimond, and C. Kervrann, “An adaptive statistical test to detect non Brownian diffusion from particle trajectories,” in *Proc. Int. Symp. on Biomedical Imaging (ISBI)*, Prague, Sloviaka, 2016, pp. 972–975.

[28] N. Chenouard *et al.*, “Objective comparison of particle tracking methods,” *Nat. Methods*, vol. 11, no. 3, pp. 281–289, Mar. 2014.

[29] Y. Kalaidzidis, “Intracellular objects tracking,” *Eur. J. Cell Biol.*, vol. 86, no. 9, pp. 569–578, 2007.

[30] E. Meijering, O. Dzyubachyk, and I. Smal, “Methods for cell and particle tracking,” *Methods Enzym.*, vol. 504, no. 9, pp. 183–200, 2012.

[31] D. Thomann, J. Dorn, P. Sorger, and G. Danuser, “Automatic fluorescent tag localization II: improvement in super-resolution by relative tracking,” *J. Microsc.*, vol. 211, no. 3, pp. 230–248, 2003.

[32] M. K. Cheezum, W. F. Walker, and W. H. Guilford, “Quantitative comparison of algorithms for tracking single fluorescent particles,” *Biophys. J.*, vol. 81, no. 4, pp. 2378–2388, 2001.

[33] I. Smal, M. Loog, W. Niessen, and E. Meijering, “Quantitative comparison of spot detection methods in fluorescence microscopy,” *IEEE Trans. Med. Imaging*, vol. 29, no. 2, pp. 282–301, 2010.

[34] C. Kervrann, C. O. S. Sorzano, S. T. Acton, J. C. Olivo-Marin, and M. Unser, “A Guided Tour of Selected Image Processing and Analysis Methods for Fluorescence and Electron Microscopy,” *IEEE J. Sel. Top. Signal Process.*, vol. 10, no. 1, pp. 6–30, Feb. 2016.

[35] R. E. Kalman and others, “A new approach to linear filtering and prediction problems,” *J. Basic Eng.*, vol. 82, no. 1, pp. 35–45, 1960.

[36] A. Genovesio, B. Zhang, and J.-C. Olivo-Marin, “Tracking of multiple fluorescent biological objects in three dimensional video microscopy,” in *Proc. Int. Conf. in Image Processing (ICIP)*, Barcelona, Spain, 2003, p. I–1105.

[37] F. Briquet-Laugier, C. Boulin, and J.-C. Olivo-Marin, “Analysis of moving biological objects in video microscopy sequences,” in *Society of Photo-Optical Instrumentation Engineers (SPIE) Conference Series*, San Jose, U.S.A., 1999, vol. 3642, pp. 4–12.

[38] B. Anderson and J. Moore, *Optimal Filtering. 1979*. Prentice-Hall, Englewood Cliffs, NJ.

[39] H. A. Blom and Y. Bar-Shalom, “The interacting multiple model algorithm for systems with Markovian switching coefficients,” *IEEE Trans Autom. Control*, vol. 33, no. 8, pp. 780–783, 1988.

[40] S. S. Blackman and R. F. Popoli, *Design and Analysis of Modern Tracking Systems*. Artech House, 1999.

[41] G. Ackerson and K. Fu, “On state estimation in switching environments,” *IEEE Trans Autom. Control*, vol. 15, no. 1, pp. 10–17, 1970.

[42] J. K. Tugnait, “Detection and estimation for abruptly changing systems,” *Automatica*, vol. 18, no. 5, pp. 607–615, 1982.

[43] M. S. Arulampalam, S. Maskell, N. Gordon, and T. Clapp, “A tutorial on particle filters for online nonlinear/non-Gaussian Bayesian tracking,” *IEEE Trans Signal Process.*, vol. 50, no. 2, pp. 174–188, 2002.

[44] H.-F. Yang, X. Descombes, C. Kervrann, C. Medioni, and F. Besse, “Tracking Growing Axons by Particle Filtering in 3D+t Fluorescent Two-Photon Microscopy Images,” in *Computer Vision – ACCV 2012*, Daejeon, Korea: Springer, 2013, pp. 272–283.

[45] M. R. Winter, C. Fang, G. Banker, B. Roysam, and A. R. Cohen, “Axonal transport analysis using Multitemporal Association Tracking,” *Int. J. Comput. Biol. Drug Des.*, vol. 5, no. 1, pp. 35–48, 2012.

[46] S. Bonneau, L. Cohen, and M. Dahan, “A multiple target approach for single quantum dot tracking,” in *Proc. Int. Symp. on Biomedical Imaging (ISBI)*, Arlington, U.S.A., 2004, pp. 664–667.

[47] K. E. Magnusson and J. Jaldén, “A batch algorithm using iterative application of the Viterbi algorithm to track cells and construct cell lineages,” in *Proc. Int. Symp. on Biomedical Imaging (ISBI)*, Barcelona, Spain, 2012, pp. 382–385.

[48] G. Kitagawa, “Non-Gaussian State-Space Modeling of Nonstationary Time Series,” *J. Am. Stat. Assoc.*, vol. 82, no. 400, pp. 1032–1041, Dec. 1987.

[49] H. E. Rauch, C. T. Striebel, and F. Tung, “Maximum likelihood estimates of linear dynamic systems,” *AIAA J.*, vol. 3, no. 8, pp. 1445–1450, 1965.

[50] D. Fraser and J. Potter, “The optimum linear smoother as a combination of two optimum linear filters,” *IEEE Trans Autom. Control*, vol. 14, no. 4, pp. 387–390, 1969.

[51] G. Kitagawa, “The two-filter formula for smoothing and an implementation of the Gaussian-sum smoother,” *Ann. Inst. Stat. Math.*, vol. 46, no. 4, pp. 605–623, Dec. 1994.

[52] M. Briers, A. Doucet, and S. Maskell, “Smoothing algorithms for state–space models,” *Ann. Inst. Stat. Math.*, vol. 62, no. 1, pp. 61–89, Jun. 2009.

[53] R. Jonker and A. Volgenant, “A shortest augmenting path algorithm for dense and sparse linear assignment problems,” *Computing*, vol. 38, no. 4, pp. 325–340, 1987.

[54] F. Aguet, C. N. Antonescu, M. Mettlen, S. L. Schmid, and G. Danuser, “Advances in Analysis of Low Signal-to-Noise Images Link Dynamin and AP2 to the Functions of an Endocytic Checkpoint,” *Dev. Cell*, vol. 26, no. 3, pp. 279–291, 2013.

[55] B. T. Helfand, L. Chang, and R. D. Goldman, “Intermediate filaments are dynamic and motile elements of cellular architecture,” *J. Cell Sci.*, vol. 117, no. Pt 2, pp. 133–141, Jan. 2004.

[56] C. J. Burckhardt, M. Suomalainen, P. Schoenenberger, K. Boucke, S. Hemmi, and U. F. Greber, “Drifting motions of the adenovirus receptor CAR and immobile integrins initiate virus uncoating and membrane lytic protein exposure,” *Cell Host Microbe*, vol. 10, no. 2, pp. 105–117, 2011.

[57] M. F. Engelke, C. J. Burckhardt, M. K. Morf, and U. F. Greber, “The dynactin complex enhances the speed of microtubule-dependent motions of adenovirus both towards and away from the nucleus,” *Viruses*, vol. 3, no. 3, pp. 233–253, Mar. 2011.

[58] F. de Chaumont *et al.*, “Icy: an open bioimage informatics platform for extended reproducible research,” *Nat. Methods*, vol. 9, no. 7, pp. 690–696, Jul. 2012.